3-2001

An Optical Survey of Outlying Ejecta in Cassiopeia A: Evidence for a Turbulent, Asymmetric Explosion

Robert A. Fesen
Dartmouth College

THE ASTROPHYSICAL JOURNAL SUPPLEMENT SERIES, 133:161–186, 2001 March

AN OPTICAL SURVEY OF OUTLYING EJECTA IN CASSIOPEIA A: EVIDENCE FOR A TURBULENT, ASYMMETRIC EXPLOSION

ROBERT A. FESEN
6127 Wilder Laboratory, Department of Physics and Astronomy, Dartmouth College, Hanover, NH 03755; fesen@snr.dartmouth.edu
Received 2000 April 20; accepted 2000 September 27

ABSTRACT

A deep optical survey of the Cassiopeia A supernova remnant has revealed dozens of new emission-line ejecta knots out beyond the remnant's bright nebular shell. Most of the newly detected knots exhibit a 4500–7500 Å spectrum dominated by [N II] $\lambda\lambda$6548,6583 line emissions. After accounting for possible decelerations, the estimated space velocities for about four dozen of these [N II] knots suggest a nearly isotropic $\simeq$10,000 km s^{-1} ejection velocity. However, a small group along the southwestern limb show significantly higher velocities of up to 12,000 km s^{-1}. Over 20 outlying O + S emission knots were also discovered, mostly along the remnant's western limb. These knots have optical spectral properties like those seen in the main shell's metal-rich "fast-moving knots" but with much higher estimated space velocities of between 7600 and 12,600 km s^{-1}. Discovery of these knots means that the remnant's highest-velocity, O + S debris are not confined to just the remnant's northeast "jet." [S II] $\lambda\lambda$6716,6731 emissions dominate the spectra of these knots above an expansion velocity of 11,000 km s^{-1}. A few "mixed emission knots," which show both strong nitrogen and sulfur line emissions, were also detected along the remnant's western rim. The properties of these outlying debris knots suggest a turbulent supernova expansion in which the innermost S-rich layers were ejected up through overlying material in certain regions, attaining final outward velocities greater than the star's N and He-rich surface layers. The detection of such high-velocity, sulfur-rich ejecta only along the remnant's northeast and southwest limbs further suggests an asymmetric expansion, possibly bipolar. A turbulent expansion may help explain the creation of the observed mixed emission knots. It is unclear, however, if mixed knots represent truly microscopically mixed debris or are simply small, comoving clusters of chemically distinct ejecta.

Subject headings: ISM: individual (Cassiopeia A) — ISM: kinematics and dynamics — supernova remnants
On-line material: machine-readable tables

1. INTRODUCTION

Studies of young Galactic supernova remnants (SNRs) offer chemical and kinematic information for supernova (SN) ejecta on much finer spatial scales than possible from either extragalactic SN or SNR investigations. Though only a small fraction of a star's ejected mass may be detectable centuries after the initial SN outburst, much still can be learned about the details of a SN's explosion dynamics by studying its ejecta fragments, particularly those with the highest velocities. The chemical composition and expansion properties of a SNR's highest-velocity, outermost ejecta can provide useful clues regarding the nature of the progenitor star, evidence for possible asymmetries of the explosion, and information on the abundances of certain key elements generated by the explosive nucleosynthesis. The physical dimensions, organization, and morphology of a SN's outer debris can also give unique empirical data on the formation and evolution of SN ejecta. In cases where sufficient circumstellar matter is present, it may also be possible to investigate a progenitor's mass-loss history and evolutionary phase just prior to outburst.

Because ejecta knots in young SNRs often possess relatively high densities and low electron temperatures ($n \sim 10^{3-4}$ cm^{-3}, $T \sim 10^{3-5}$ K), optical investigations are a particularly useful means for exploring clumps of ejecta. High-velocity knots of SN debris can be shock-excited and ionized, and thus made optically visible, as they interact with either the main and reverse shocks or with the surrounding interstellar medium.

With a current age of $\simeq$320 yr, the remnant Cassiopeia A (Cas A) is the youngest Galactic SNR known. Quickly recognized as being the brightest radio source in the northern sky at low frequencies (Reber 1944; Ryle & Smith 1948), coincident optical emission was soon identified by Baade & Minkowski (1954). Finding numerous optical filaments with radial velocities $\geq$3000 km s^{-1}, large internal motions, and unusual line ratios, they surprisingly did not recognize it at first as a young supernova remnant despite prior suggestions along those lines (Parenago & Shklovsky 1952; Shklovsky 1953). Subsequent optical studies revealed it to be a remarkable SNR in terms of its chemical and kinematic properties (Minkowski 1959, 1968; van den Bergh 1971; Peimbert & van den Bergh 1971).

There is now considerable evidence from optical, infrared, and X-ray abundance analysis that Cas A is the remnant of a massive star (Chevalier & Kirshner 1978, 1979; Tsunemi et al. 1986; Jansen et al. 1988; Douvion et al. 1999). A WN-type Wolf-Rayet star of mass 10–30 $M_\odot$ has been most often suggested as the likely progenitor (Langer & El Eid 1986; Fesen, Becker, & Blair 1987; Fesen, Becker, & Goodrich 1988; García-Segura, Langer, & Mac Low 1996), with indications for a high, pre-SN mass-loss rate (Vink, Kaastra, & Bleeker 1996).

An estimated explosion date of A.D. 1658 $\pm$ 3 yr was derived from extensive, multiyear studies of its expanding bright optical nebulosity (Kamper & van den Bergh 1976; van den Bergh & Kamper 1983). However, the Cas A supernova outburst may have actually been sighted by Flamsteed

in A.D. 1680 (Ashworth 1980). This later date is more consistent with estimates of around 1671–1677 based on studies of the remnant's less decelerated, outer knots (Kamper & van den Bergh 1976; Fesen, Becker, & Blair 1987, hereafter FBB87; Fesen, Becker, & Goodrich 1988, hereafter FBG88).

Located at $l = 111.^{\circ}7, b = -2.^{\circ}1$ and lying at an estimated distance of $3.4^{+0.3}_{-0.1}$ kpc (Reed et al. 1995; thus $1' = 0.99$ pc), Cas A appears as a $\simeq 2$ pc radius shell of bright emission possessing several distinctive types of optical knots (see Table 1). Large proper motion, high radial velocity ejecta called "fast-moving knots" (FMKs; $v = 4000$–6000 km s^{-1}) show strong O, S, and Ar lines but no H, He, or N emissions, suggesting these are debris fragments from the supernova's mantle and core. Much slower moving, semi-stellar knots called "quasi-stationary flocculi" (QSFs; $v \leq 400$ km s^{-1}) show both hydrogen Balmer emission and strong [N II] lines consistent with them being CNO processed, circumstellar mass-loss material (CSM). Faint, high-proper motion [N II] $\lambda\lambda$6548,6583 emission dominated knots ($v = 7000$–9000 km s^{-1}) have also recently been found along the remnant's outer boundary. Like the QSFs, these knots appear to be debris from the progenitor's N and He rich outer layers. Because the first few of these knots showed line strengths like those seen in the QSFs, FBB called these "fast-moving flocculi" (FMFs). However, since most do not show any optical emission other than nitrogen, we will simply refer to them as nitrogen knots or "NKs." A handful of so-called "mixed-emission knots" (MEKs) have also been found which show [N II] emissions and high proper motions like NKs while also having strong O, S, and Ar emissions like the FMKs.

Despite a relatively high line-of-sight extinction in the optical ($A_V = 5$–6 mag or more; Searle 1971; Hurford & Fesen 1996), Cas A offers perhaps the best opportunity for an in-depth, high-resolution study of a young SNR resulting from the explosion of a high-mass progenitor, i.e., a SN II or SN Ib,c. Indeed, past investigations into Cas A's high-velocity ejecta have already yielded considerable detailed information on the range of ejecta knot velocities and SN ejecta abundances (Peimbert & van den Bergh 1971; Kirshner & Chevalier 1977; Chevalier & Kirshner 1978, 1979; van den Bergh & Kamper 1983, 1985).

Insights into the remnant's kinematics and expansion asymmetry have come from recent research on the remnant's fastest-moving, outermost knots (FBB87; FBG88). These studies have indicated that the Cas A progenitor may have had a N-rich photosphere at time of outburst with the presence of hydrogen in a handful of detected outer knots, raising the possibility of an early, albeit brief, Type II spectroscopic phase (Fesen & Backer 1991) like that seen in some Type II/Ib SNe (e.g., SN 1987K, SN 1993J; see Filippenko 1997). In addition, the remnant's northeastern "flare" or "jet" of exceptionally high-velocity, sulfur bright knots suggests a possible asymmetry in the Cas A SN explosion in which underlying S-rich material was ejected with velocities much greater than that of the photospheric debris (van den Bergh 1971; Fesen & Gunderson 1996, hereafter FG96; Fesen & Becker 1991, hereafter FB91). Finally, the detection of a few "mixed" emission knots indicated progenitor layer mixing during the SN explosion in the region of the jet (FB91).

Unfortunately, no systematic optical survey of the remnant's outer, high-velocity knots has been undertaken to date. Previous studies employed narrow Hα and [S II] interference filters and consequently could have easily missed outer knots having large radial velocities ($|v| \geq 2000$ km s^{-1}). Prior searches also looked specifically for Hα or [N II] emitting ejecta (i.e., NK knots), with the result that faint, high-velocity S and O emitting FMKs could have gone undetected.

In this paper, the results of a more comprehensive reconnaissance of Cas A's outermost optical emission knots are presented. This survey has resulted in the discovery of dozens of additional outlying knots, which in turn has revealed further details about the core-collapse dynamics of the Cas A supernova.

2. OBSERVATIONS

2.1. *Imaging*

With the objective of surveying the population of faint, outlying line emission knots around the remnant, several sets of deep interference-filter images of Cas A were obtained in 1996 October using a 1024 × 1024 Tektronix CCD detector attached to the Hiltner 2.4 m telescope at the Michigan-Dartmouth-MIT (MDM) Observatory. The telescope-camera system produced a 4.′7 square field of view with 0.″275 pixels. The remnant's limb was divided into four imaging quadrants (NE, SE, NW, and SW) so as to cover an expansion velocity distance from remnant center equivalent to roughly twice the ~ 6000 km s^{-1} of the remnant's main shell.

Filters were chosen that would allow the detection of knot emission lines at both large positive and negative radial velocities. These included Hα (FWHM = 90 Å) to detect [N II] $\lambda\lambda$6548,6583 emitting knots with low to moderate radial velocities ($v_r \pm 2000$ km s^{-1}), a 6450 Å filter (FWHM = 90 Å) for negative velocity [N II] emitting ejecta ($v_r = -4000$ to -7500 km s^{-1}), a broad 6650 Å filter (FWHM = 250 Å) to detect both [S II] $\lambda\lambda$6716,6731 emission knots with $v_r = -4000$ to $+3000$ km s^{-1} and [N II] knots with large positive velocities ($v_r = +1000$ to $+8500$ km s^{-1}), and a standard *R*-band filter to serve as a reference on stellar sources in each field. The southeastern rim of the remnant was also imaged using 6100 Å and 6300 Å filters (FWHM = 100 Å) to investigate the presence of a few [O I] emitting knots in this area that were serendipitously dis-

TABLE 1

OPTICAL KNOT TYPES IN CASSIOPEIA A

Knot Type	Abbreviation	Dominate Optical Emission Lines	Nature
Fast-moving knots	FMK	[S II], [S III], [O I], [O II], [O III], [Ar III]	SN ejecta
Quasi-stationary flocculi.....	QSF	[N II], Hα	Circumstellar
Nitrogen knots	NK	[N II]	SN ejecta
Mixed emission knots.....	MEK	[N II], [S II], [S III], [O I], [O II], [O III], [Ar III]	SN ejecta

covered spectroscopically in an earlier study (FG96). Usually, two exposures of between 600 and 1000 s were taken in each filter for the four fields, with each image set co-added, bias subtracted, and dome or sky flat corrected. Typical seeing varied between 1″ and 2″ (FWHM).

Additional images were taken in 1998 September using the same telescope but this time using a 2048 × 2048 SITe CCD, producing a 9′ FOV with 0.″275 pixels. Three 2000 s exposures of the remnant and vicinity were taken using a narrow Hα filter (FWHM = 30 Å) and a matched continuum filter centered at 6510 Å. The Hα image detected both QSF emission and faint diffuse H II emission, while a comparison with the 6510 Å image revealed the presence of a few blueshifted NK-type knots along the north and east limbs.

2.2. *Spectroscopy*

Low-dispersion optical spectra of known or suspected outlying emission knots were obtained on three nights in 1996 October using the MDM 2.4 m telescope with the Mark III Spectrograph and a 1024 × 1024 Tektronix CCD detector. A 1.″2 × 4.′5 slit and a 300 lines mm^{-1} 5400 Å blaze grism were used to obtain sets of two or three 1000–1200 s exposures spanning the spectral region 4500–7400 Å with a spectral resolution of $\simeq 8$ Å. A N-S slit was typically used except in cases like Knots 21A, 21B, and 21C in the northeast, where we employed a NE-SW slit (position angle = 23.°5) to obtain several knot spectra at once.

Spectral data were reduced using standard IRAF software routines and calibrated with Hg, Ne, and Xe lamps and three to four Oke (1974), Stone (1977), or Massey & Gronwald (1990) standard stars. All three nights were photometric. However, with seeing only between 1″ and 1.″5, slit light losses were at times considerable, sometimes resulting in lower measured knot fluxes relative to previous measurements (e.g., for NK 15). Also, due to unexpectantly large spectrograph flexure during the run, measured radial velocities were later checked and corrected using night-sky lines as zero-velocity reference points (Osterbrock & Martel 1992). Radial velocities are believed accurate to ± 100 km s^{-1}, affected as much by the low dispersion as by the blind offsets used and hence uncertainties in precise knot locations within the slit. Flux measurement errors can reach 50% due to uncertainties in knot locations in the slit. Weak residue night-sky emissions at [O I] λ5577 and λ6300 due to imperfect sky subtraction were manually removed in the final reduced spectra.

Additional radial velocity measurements on several knots (including Knots 6A, 14A, 15A, 15C, and 23–27) were obtained on several nonphotometric nights during 1997 May and June and 1998 October using the 2.4 m MDM telescope. For these data, a Modular Spectrograph was used together with a 600 lines mm^{-1} 5000 Å blaze grating and a 1.″5 wide slit. Data reduction was similar to that of the 1996 October data, but with radial velocity measurement uncertainties of ± 75 km s^{-1}.

3. RESULTS

Our survey of Cas A uncovered nearly four dozen new optical emission knots in the outskirts of this well studied remnant. These include 25 new [N II] λλ6548,6583 knots (NKs). This brings the total number of such high-speed knots in the outskirts of Cas A now to 50, up from the 15 cited by FBG88 in 1988 plus the nine later found in the NE jet region (FG96). The survey also uncovered 19 new outlying FMKs. These FMKs are the first outlying knots to be found outside of the northeast jet region. In fact, most of these new FMKs are located along Cas A's western rim roughly opposite from the jet. This indicates a much wider distribution of high-velocity O + S debris than previously realized. In addition, three "mixed emission knots" (MEKs) were also detected outside the remnant's western rim.

A finding chart for the outer Cas A knots discussed in this paper is shown in Figure 1. Marked are 49 of the 50 currently known NKs (NK 13 has faded since its detection by FBG88) along with 19 FMKs (excluding jet FMKs; see Fesen & Gunderson 1996) and 6 MEKs. Small regional finding charts are presented in Figures 2*a*–2*o*. Although we chose finder chart images which showed the majority of emission knots best in each region, some knots appear only faintly (or even entirely absent) on these images due to their large radial velocities shifting their principal emission lines out of the filter's bandpass.

The naming convention adopted for the newly discovered knots was to identify them with an already known nearby knot, usually by adding a letter. This worked well in several cases (e.g., Knots 3, 3A–B; 12, 12A–12E) but grew elaborate in others (e.g., Knots 19, 19A–19M). However, nothing more than a need to name an ever increasing population of outer knots is implied by these knot identification names. Because both the discovery and subsequent spectroscopic confirmation did not always follow a prescribed or orderly manner, the resulting knot identification numbers do not follow a pattern or change systematically around the remnant. Brief comments on some individual knots is given in Appendix A.

3.1. *Outlying* [N II] *Dominated Debris* (*NKs*)

Low-dispersion optical spectra of two of the brighter NK knots, Knots 12 and 15, are shown in Figures 3*a* and 3*b*, respectively. These spectra are representative of the majority of NK knots in that they show a 4500–7500 Å spectrum dominated by the two [N II] λλ6548,6583 lines.

Our spectrum of NK 15 is similar to that obtained by FB91, except that we find no evidence for weak He I λ5876 emission which would be shifted to 5964 Å ($v_r = +4500$ km s^{-1}). With just the two [N II] lines present in this low-dispersion spectra, it is difficult to determine much in the way of knot physical properties such as electron density or internal velocity dispersion. However, adopting an $E(B-V) = 1.6$ (Hurford & Fesen 1996), the lack of detectable emission from the temperature sensitive [N II] λ5755 line [i.e., $I(6583 + 6548)/I(5755) \geq 40$] suggests $T_e \leq 16{,}000$ K assuming $N_e \leq 5000$ cm^{-3}.

For Knots 12 and 15, like nearly all NK spectra, Hα is substantially weaker relative to the [N II] lines when compared to that seen in the remnant's circumstellar QSFs. In Table 2, we list observed values or lower limits for the [N II] λ6583/Hα line ratio for 38 of the 50 NKs. For most NKs, Hα emission was undetected due to either intrinsically weak Hα flux (i.e., [N II] λ6583/Hα ≥ 3) and/or low S/N data. For 18 knots, we could set a lower limit of [N II] λ6583/Hα ≥ 5. For the brightest NKs where relatively good S/N data were obtained, weak Hα emission was seen (e.g., Knots 10, 13B, 15, and 15A). The most extreme case is for the bright knot Knot 15 ("KB 91," Kamper & van den Bergh 1976) where

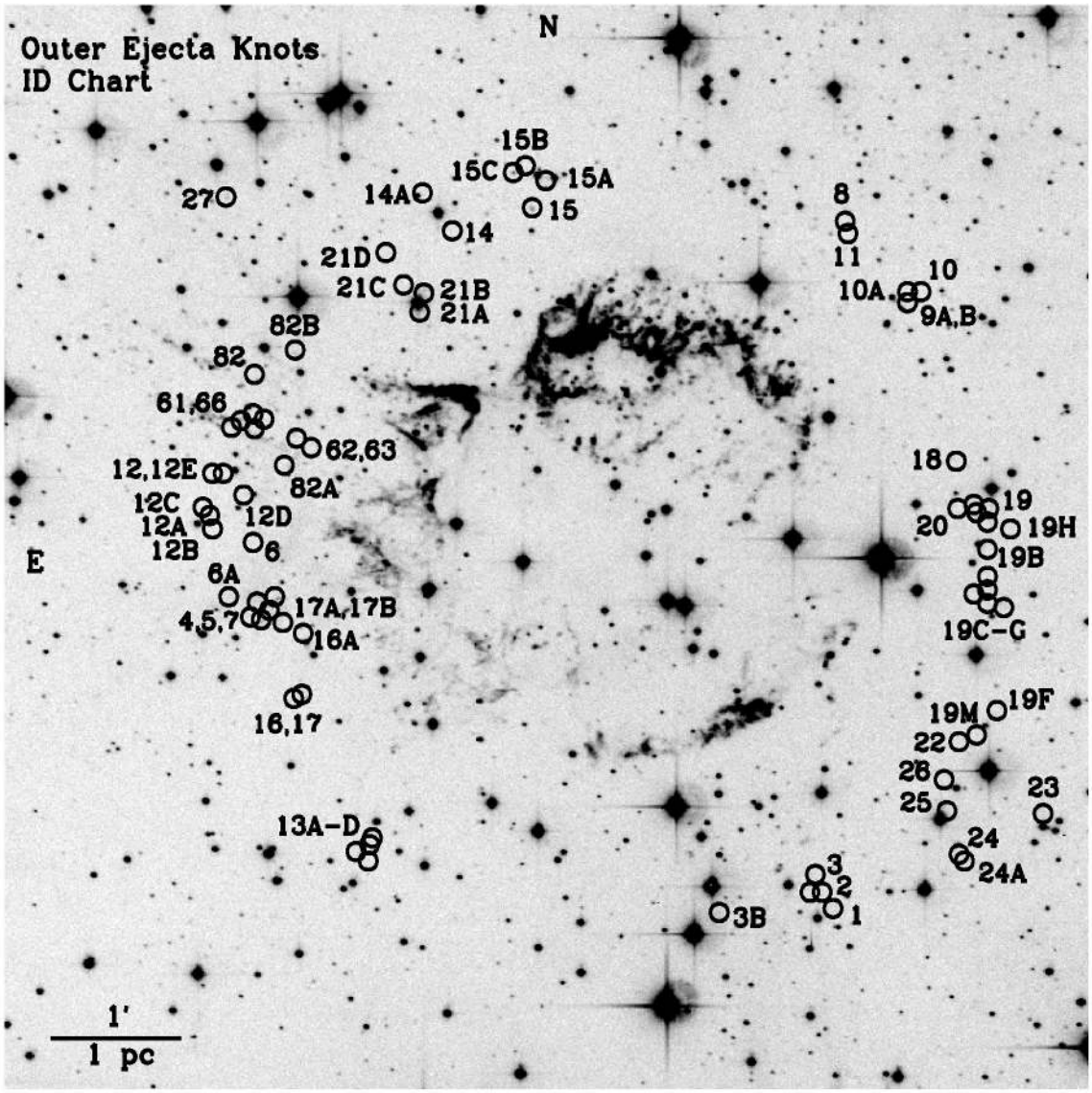

FIG. 1.—Outer ejecta knot identification chart. Image is a [S II] λλ6716,6731 CCD frame of Cas A taken in 1992 (Fesen & Gunderson 1996). Locations of over 70 knots for epoch 1996–1998 are marked.

the [N II] λ6583 emission was detected with an intensity some 30 times that of Hα.

Large [N II] λ6583/Hα ratios are in sharp contrast to those seen in the slower moving, circumstellar QSFs which exhibit $I(\mathrm{H}\alpha) \simeq 0.3 \times I([\mathrm{N\ II}]\ \lambda 6583)$ (van den Bergh 1971; Chevalier & Kirshner 1978; Hurford & Fesen 1996). The only exceptions to this rule are three NK knots located in the remnant's southwest region (NKs 1–3) which do show QSF-like Hα line strengths (see spectra in FBB87).

The [N II] λ6583 flux threshold for our NK detection was $\simeq 1 \times 10^{-16}$ erg cm^{-2} s^{-1}, with an average [N II] λ6583 flux of around 3×10^{-16} erg cm^{-2} s^{-1} for the knots detected. The brightest ones (Knots 6 and 15) exhibited [N II] λ6583 fluxes around 1×10^{-15} erg cm^{-2} s^{-1} and can be seen on a few broadband archival 1951–1985 Palomar 5 m plates published in the literature (Kamper & van den Bergh 1976; FBB87).

We note the [N II] emission fluxes listed in Table 2 must be viewed with caution. Knot emission fluxes are known to change significantly with time (Kamper & van den Bergh 1976). In addition, the observed values are subject to errors up to 50% due to varying seeing conditions and slit placement errors due to the blind-offset procedure employed in obtaining the spectra.

Table 2 also lists observed radial and estimated average transverse velocity data for all 50 known NKs, combining previous kinematic and line flux NK information from FBB87, FBG88, and FB91. Time-averaged transverse velocities for individual knots were estimated using currently observed displacements from the remnant's estimated center of expansion (Kamper & van den Bergh 1976) and assuming a remnant distance of 3.4 kpc and an explosion date of A.D. 1680. For about half a dozen knots where spectroscopic data were not available, approximate radial velocities (± 1000 km s^{-1}) were estimated based upon knot detectability in various narrow passband filter images assuming [N II] λ6583 dominated the optical spectrum. In these few cases, a NK nature was suggested either by detection on Hα or Hα continuum images (6510 Å, FWHM = 30 Å, or 6450 Å, FWHM = 90 Å). Because the transverse

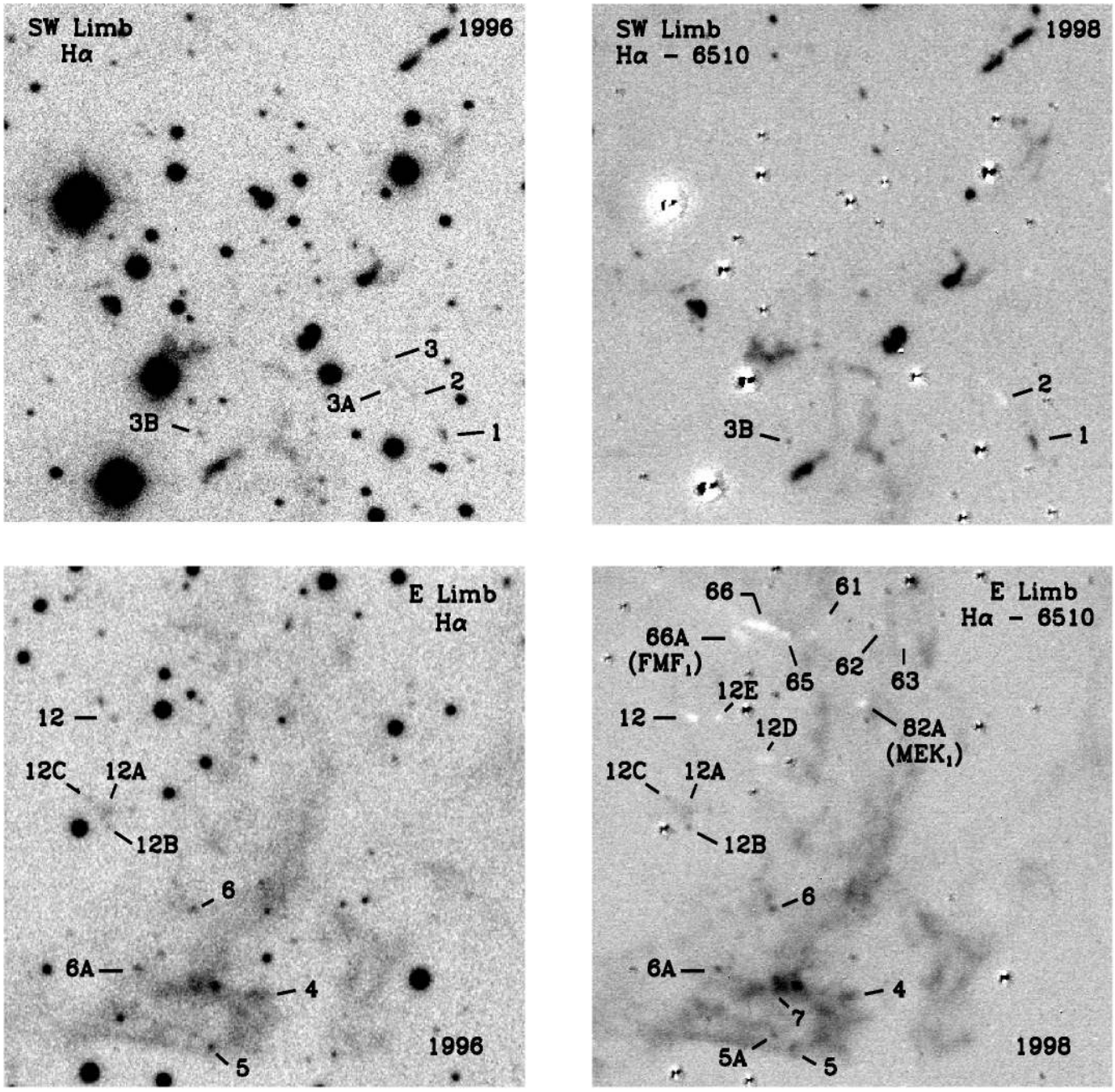

FIG. 2.—(*a*–*o*) Finder charts (FOV = 110′ × 110′) for outlying Cas A ejecta discussed in this paper. The specific remnant limb region, filter bandpass of the image, and the year the image was obtained are indicated on each chart. Due to large radial velocities of some ejecta within a given area, a few knots appear faint or entirely absent on some frames. Panels (*b*), (*d*), and (*h*) are Hα minus 6510 Å continuum subtracted images in which blueshifted nitrogen emission knots (i.e., those appearing only on the 6510 Å image) appear as white (rather than dark) features in the figures.

velocities for these knots are large ($v_t \geq 8400$ km s^{-1}), uncertainty in their derived space velocities is relatively small.

Our NK velocity data reveal radial velocities ranging from +5670 km s^{-1} (Knot 14) to −6530 km s^{-1} (Knot 21A). Interestingly, this spread is about equal to the maximum expansion velocity of the remnant's bright ejecta shell (Reed et al. 1995) despite knot locations well outside the main remnant shell. Estimated average transverse velocities range from 7300 to 11,600 km s^{-1} with most lying between 7500 and 10,000 km s^{-1}.

Despite a wide range of both radial and inferred transverse velocities, the currently known NKs exhibit space velocities between 8100 and 12,000 km s^{-1} (rounded to the nearest 100 km s^{-1}), with all but two (Knots 24 and 24A in the SW) within 8100–10,600 km s^{-1}. This is shown graphically in Figure 4. This suggests a relatively uniform expansion velocity for Cas A's strong nitrogen emission ejecta near the plane of the sky, especially when compared to that seen for the O, S, Ar emission FMKs (see § 3.4 below).

However, as can be seen in Figure 5, the projected positions of the currently known NKs are not entirely isotropic.

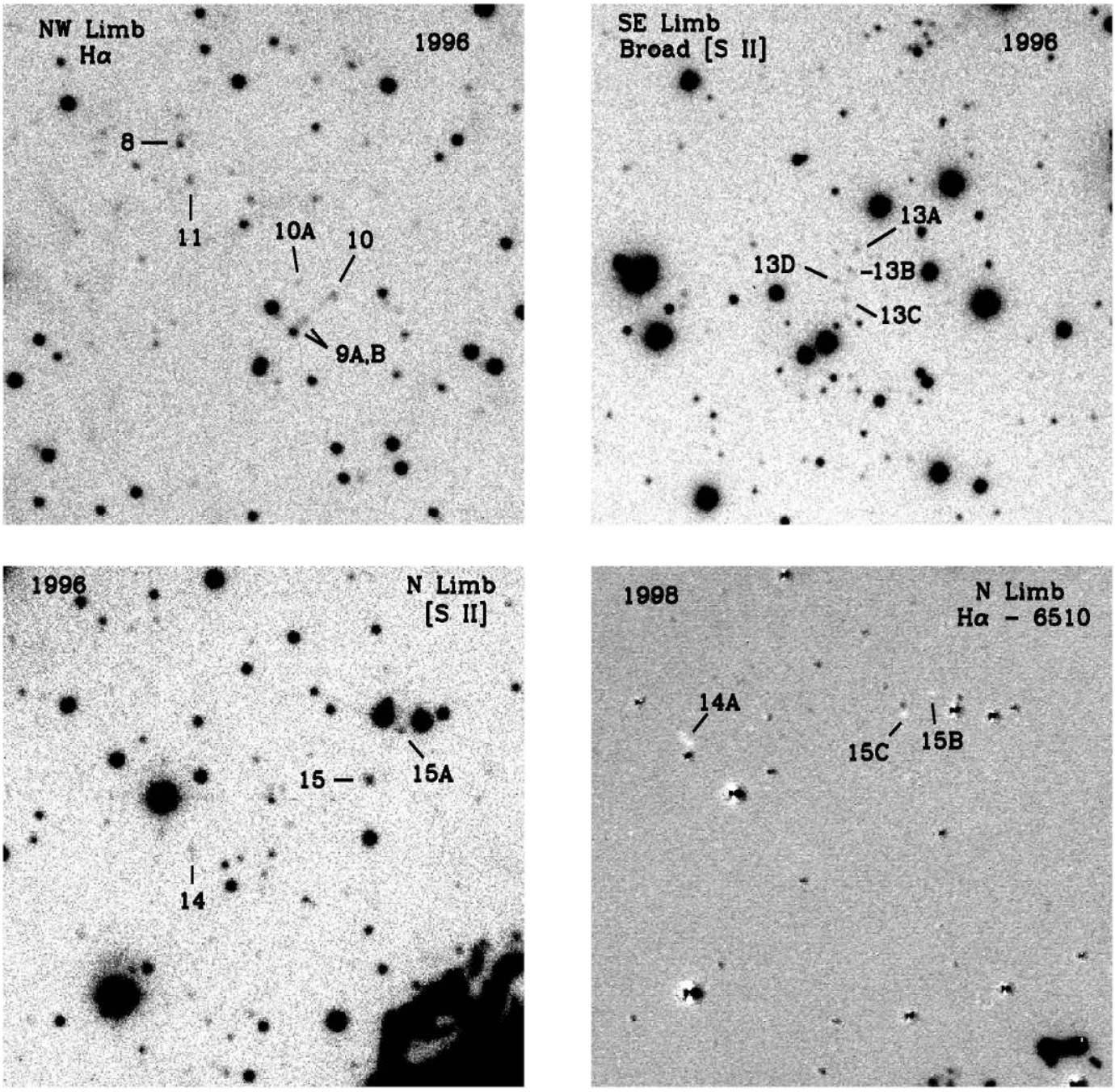

FIG. 2.—*Continued*

Although the NKs (filled circles) are detected along much of the remnant's periphery, even in the northeast jet region, there are two large opposing areas devoid of NK knots along in the NNW and SSE rims. Combined, these void regions represent about a fourth of the remnant's perimeter. A lack of NKs in these areas appears real since these sections were well covered in the overlapping NE/NW and SE/SW imaging frames. Moreover, a concerted effort was made to search for knots of any type in these regions once these empty limb areas were recognized. A possible explanation for the NNW gap is discussed in § 4.3 below.

In outlying regions where several NKs were detected, small localized groups or clusters were often seen (e.g., NKs 1–3A, 8–10A, 13A–D, and 60–65). Individual knots in these clusters tend to have similar radial and total space velocities. Examples are the neighboring knots of NK 13B, 13C, and 13D which have nearly identical radial velocities. Another particularly interesting case is that of Knots 21A–21D which show an orderly progression of radial velocity and radial displacement ($v_r = -6530, -6070, -5550, -4950$ km s^{-1}, $v_t = 6800, 7300, 7800, 8700$ km s^{-1}) leading these four knots to have nearly identical space velocities of $\simeq 9500$ km s^{-1}.

3.2. *Outlying* O *and* S *Emission Debris* (*FMKs*)

Apart from the FMKs in the northeastern jet, there had never been any FMKs found outside Cas A's main shell. However, our survey discovered 19 (see Table 3). As shown in Figure 5, most of these nonjet FMKs lie along the remnant's western and southwestern limbs (Knots 19A–

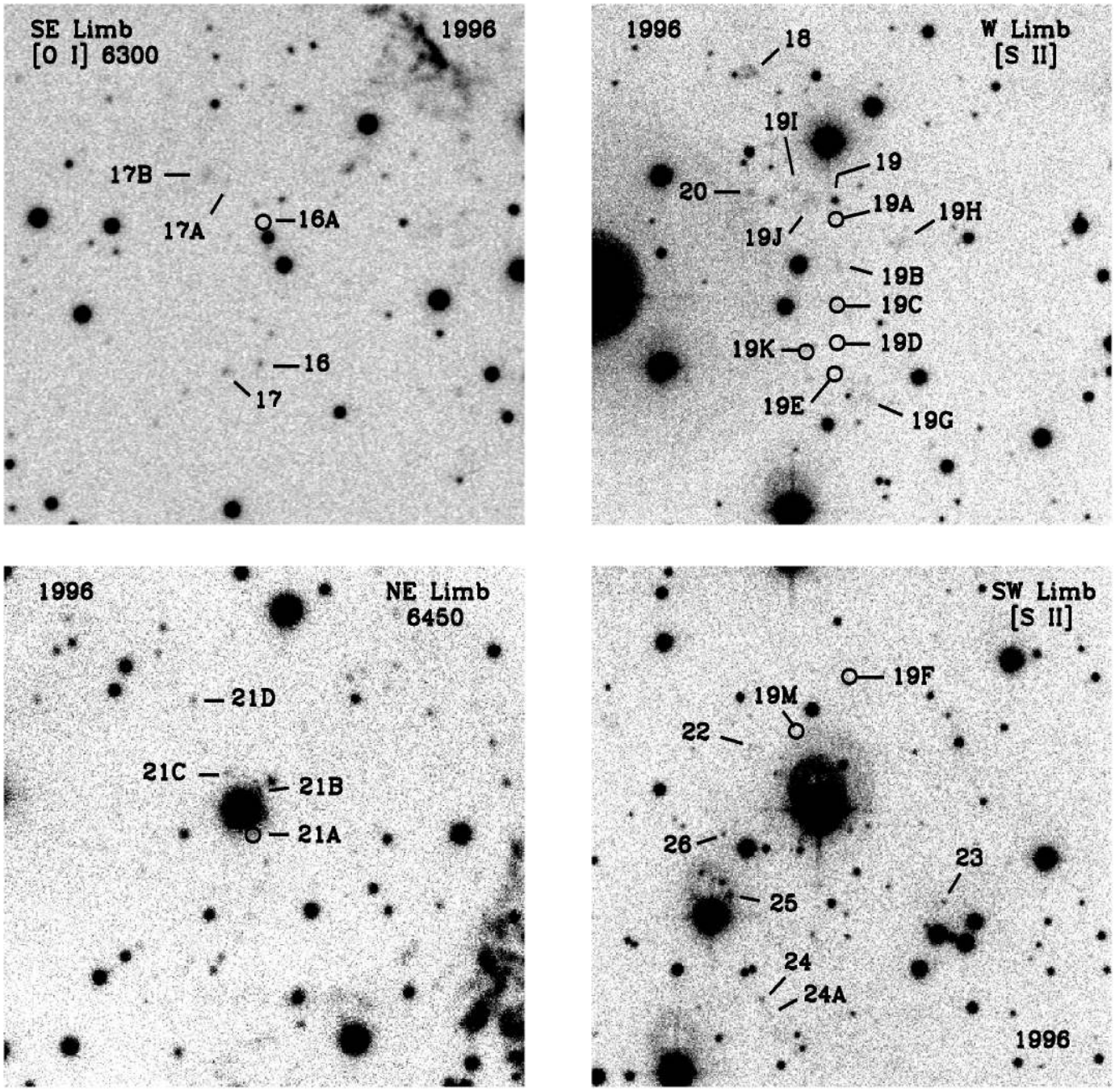

FIG. 2.—*Continued*

19M, 22, and 23), with four others located in the east and southeast (Knots 16, 17–17B) and one lone knot (Knot 27) in the northeast which might be just an errant jet FMK. The high density of FMKs along the western limb, many of which were found accidently through long slit spectra, suggests many more faint FMKs may exist in this region.

Except for FMK Knots 17B and 19J, spectra were obtained on all the new outlying FMKs. Table 3 lists observed radial and inferred transverse and space velocities for all 19 new FMKs, along with spectral line fluxes where available. As was found in the case of the strong [N II] knots, radial velocities span a wide range, from -1000 to $+5500$ km s^{-1}. Inferred space velocities lie between 7600 and 12,600 km s^{-1}, with the highest values found both in the southwest (Knots 19F and 23: 11,200–12,600 km s^{-1}) and in the northeast (Knot 27: 12,500 km s^{-1}) just above of the northeast jet. Conversely, the southeast Knots 16–17B have the lowest estimated space velocities ($\simeq$7600–8200 km s^{-1}), placing them kinematically just outside the 6000 km s^{-1} expansion velocity of the main shell's rear hemisphere (Reed et al. 1995) and inside the slowest NKs (8000–8500 km s^{-1}; Table 1).

Figures 6*a*–6*d* show spectra of four newly detected outer FMKs and illustrate some of their emission line diversity. The relatively slow-moving Knots 16 and 17, which lie just outside Cas A's SE rim (see Figs. 1 and 2*i*), exhibit spectra not unlike those seen in the remnant's main shell (Hurford & Fesen 1996), namely bright O and S lines (Knot 16, Fig. 6*a*) and an oxygen dominated spectrum (Knot 17, Fig. 6*b*). However, these two knots are quite unlike most newly dis-

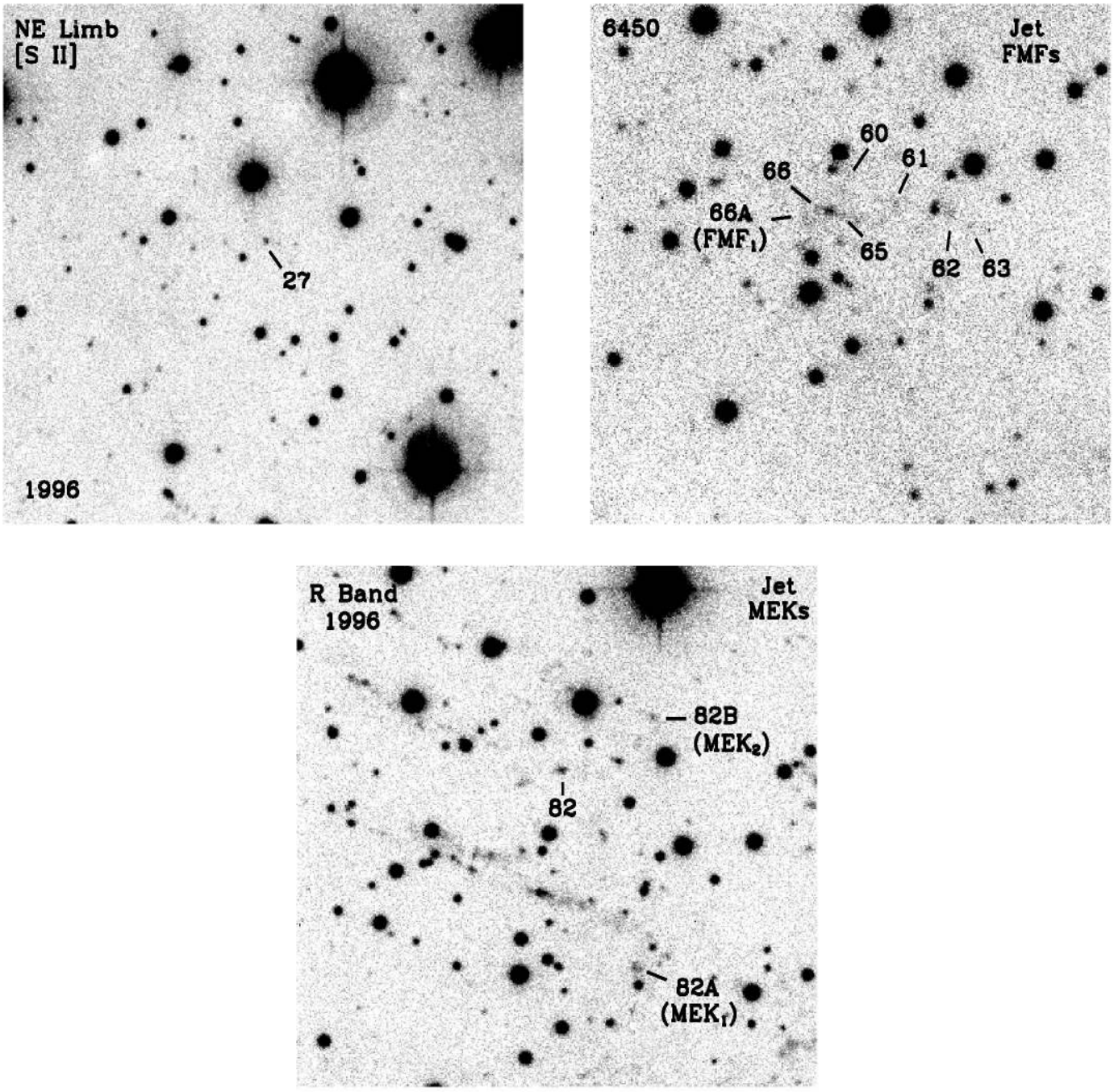

FIG. 2.—*Continued*

covered outer FMKs, where [S II] $\lambda\lambda$6716,6731 is the dominant line emission and where lines of oxygen are virtually absent (e.g., Knots 22 and 27; Figs. 6*c* and 6*d*).

3.3. *Mixed Emission Knots* (*MEKs*)

The first "mixed emission knot" in Cas A was reported by FB91 who found one bright knot in the jet region showing both Hα and [N II] emissions like NKs/QSFs, and O and S lines like those seen in FMKs. About a dozen additional jet knots were subsequently found to have QSF/FMK mixed emission properties to varying degrees (FG96).

Our study uncovered three additional MEK type knots, all located along the remnant's western limb (Knots 18, 19, and 20; see Fig. 5 and ID charts Figs. 1 and 2*j*). These knots lie among the newly discovered western FMKs, on the opposite side of the remnant from the NE jet, the only previously known region having MEK type knots. Figures 7*a*–7*d* show spectra of two of these western MEKs (18 and 19) along with spectra of two jet MEKs (82A and 82B; see ID charts Figs. 1 and 2*o*) discovered by FG96 for comparison. In the spectrum of Knot 18, the [N II] emission is weak compared to the O, S, Ar lines, whereas the [N II] lines dominate the optical spectrum of Knot 19, as they do in the spectra of some jet MEKs. No Hα emission was seen in any of these three new MEKs.

Table 4 lists observed radial and inferred transverse and space velocities for the three new western limb MEKs along

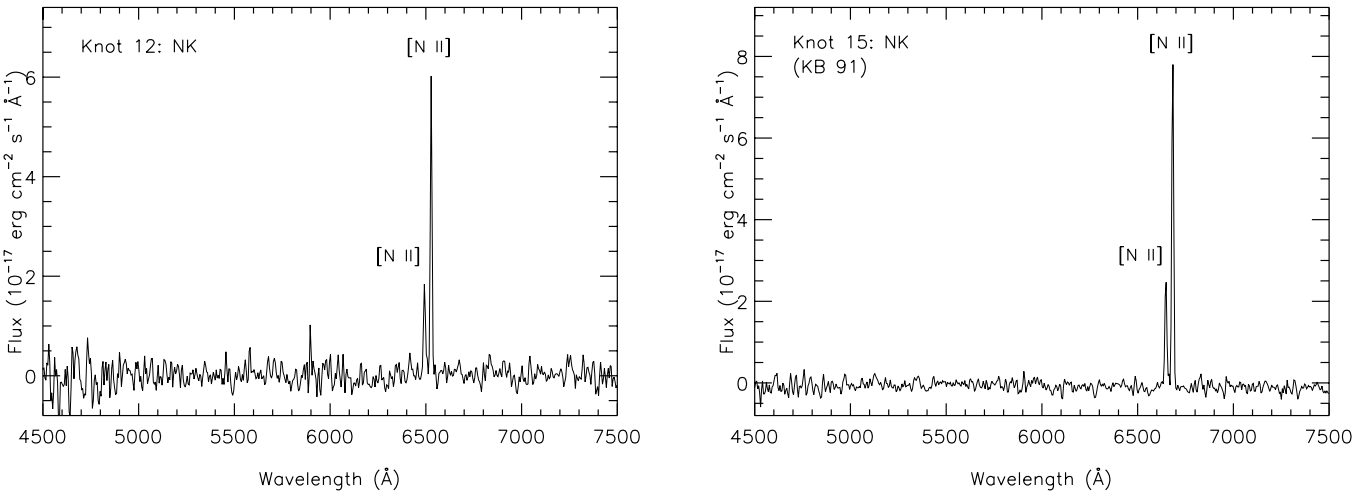

FIG. 3.—Spectra of two representative high-velocity, nitrogen-dominated, ejecta knots (NKs) in Cas A

with three jet MEKs. Although all line emissions observed in each knot exhibit, within measurement accuracy, the same radial velocities, the true nature of these "mixed" ejecta is uncertain. Knot 18, for example, can be seen in Figure 2*j* to be resolved into several individual knots. The same is true for Knot 82A in the jet (see Fig. 2*o*) and maybe even the prototype knot 82 discussed by FB91. Higher spatial resolution images along with follow-up spectra will be needed to determine whether these knots are homogeneously mixed ejecta or simply closely packed clusters of chemically distinct NK/FMK debris.

With so few MEK type knots detected, little can be said about their overall kinematic properties. Both the western limb and jet MEKs listed here exhibit similar space velocities of around 9000–10,000 km s^{-1}. However, 11 other jet MEKs show a somewhat larger space velocity range of 8500–12,000 km s^{-1} (FG96; Appendix B). The inferred electron densities these six MEKs range from 4000 to 16,000 cm^{-3}, with the [S II] 6716/6731 ratio often close to the high-density limit of 0.46.

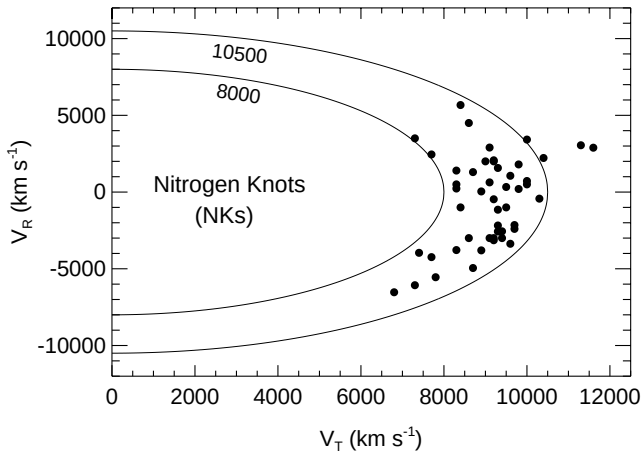

FIG. 4.—Plot of observed radial velocity (V_R) vs. inferred transverse velocity (V_T assuming $d = 3.4$ kpc and t_{SN} = A.D. 1680) for 50 nitrogen-dominated emission knots (NKs). Solid curves show space velocity loci for 8000 and 10,500 km s^{-1}. The four knots lying outside of the 10,500 km s^{-1} velocity line are all from the remnant's southwest quadrant.

3.4. *Projected Space Velocities*

Space velocities for individual knots were calculated using observed or inferred radial velocities together with estimated average transverse velocities. Transverse velocities were determined by a knot's radial displacement from Cas A's center of expansion as derived by Kamper & van den Bergh (1976) assuming a remnant distance of 3.4 kpc and an explosion date of A.D. 1680. Resulting knot space velocities are listed in Tables 2–4.

A comparison of space velocity histograms using 500 km s^{-1} bins for the three different types of outer ejecta knots is shown in Figure 8. The 50 [N II] strong NKs and the 19 O + S strong FMKs have a similar space velocity range, namely 7500–12,500 km s^{-1}. However, NKs show a somewhat bell-shaped distribution peaked at around 9500 km s^{-1}, while the FMKs have a relatively flat velocity distribution. Although MEKs have a velocity range that matches the overlap region for FMKs with the distribution peak for the NKs, no meaningful statement about their overall expansion velocities can be made from a sample of only six knots.

A plot of NK derived projected angular displacements from the remnant's nominal center (Kamper & van den Bergh 1976) using NK estimated space velocities is shown in Figure 9*a*. The solid circle represents the radial displacement for a 320 yr averaged space velocity of 10,000 km s^{-1} in all directions. This figure reveals a surprising uniformity of NK ejection velocities around 10,000 km s^{-1}, especially along the northern limb.

Strong, systematic deviations from this 10,000 km s^{-1} velocity circle can be seen along the eastern limb, however, where all NKs have space velocities under 10,000 km s^{-1}. The remnant's eastern limb region contains (in projection) a relatively bright, diffuse cloud visible on deep *R*-band or Hα images (van den Bergh & Kamper 1983; Lawrence et al. 1995; FG96) like that shown in Figure 10. This emission is likely that of an H II region due to its strong Hα and relatively weak [S II] emission (FBB87; Lawrence et al. 1995). If this cloud lies physically along the eastern limb of the Cas A SNR, NKs here might experience significant deceleration as they interact with this cloud, resulting in the lower expansion velocities seen in this region. If this is the case, it raises the possibility of a nearly isotropic NK

TABLE 2

HIGH-VELOCITY, [N II] λλ6548,6583 DOMINATED EJECTA KNOTS (NKs)

Knot ID	Limb Area	R[a] (arcsec)	$\langle\mu\rangle$[b] (arcsec yr^{-1})	V_T[c] (km s^{-1})	V_R (km s^{-1})	V_{Space} (km s^{-1})	λ6583/Hα	λ6583 Flux[d]	Refs.
1	SW	202	0.64	10300	−430	10300	4	...	1, 6
2	SW	191	0.60	9700	−2150	10000	3	...	1, 6
3	SW	182	0.58	9300	−2180	9500	3	...	1, 6
3A	SW	187	0.59	9500	+330	9500	≥3	2.3	6
3B	SW	178	0.56	9100	+630	9100	≥1	...	6
4	E	151	0.48	7700	+2450	8100	≥6	...	1, 6
5	E	162	0.51	8300	+1400	8400	≥10	...	1, 6
5A	E	165	0.52	8400	0 to −2000	∼8500	...	...	6
6	E	163	0.52	8300	+230	8300	≥6	8.0	1, 6
6A	E	175	0.55	8900	+40	8900	≥2	...	1, 6
7	E	164	0.52	8300	+400	8300	...	...	1, 6
8	NW	196	0.62	10000	+500	10000	≥10	...	1,2, 6
9A,B	NW	188	0.59	9600	+1060	9600	≥15	...	1, 2, 6
10	NW	196	0.62	10000	+750	10000	≃7	...	2, 6
10A	NW	193	0.61	9800	+1800	10000	≥3	...	6
11	NW	192	0.61	9800	+200	9800	≥1	...	2, 6
12	E	184	0.58	9400	−2560	9700	≥10	6.1	2, 6
12A	E	182	0.58	9300	−1150	9400	≥4	3.4	6
12B	E	182	0.58	9300	−470	9300	≥3	1.2	6
12C	E	187	0.59	9500	0 to −2000	∼9500	...	...	6
12D	E	168	0.53	8600	−2000 to −4000	∼9100	...	...	6
12E	E	179	0.57	9200	−2000 to −4000	∼9700	...	...	6
13	SE	180	0.58	9300	+1570	9400	≥6	...	2
13A	SE	171	0.54	8700	+1300	8800	≥4	≃4.5	6
13B	SE	176	0.56	9000	+2000	9200	≃15	5.9	6
13C	SE	181	0.57	9200	+2000	9400	≥3	2.2	6
13D	SE	180	0.57	9200	+2070	9400	≥4	2.3	6
14	NE	166	0.52	8400	+5670	10100	≥4	1.1	2, 6
14A	NE	191	0.60	9700	−2400	10000	≥7	...	6
15	N	168	0.53	8600	+4500	9700	≃30	9.5	2, 3, 4, 6
15A	N	178	0.56	9100	+2950	9600	≃11	5.0	6
15B	N	186	0.58	9500	−2000 to −4000	∼9900	...	...	6
15C	N	183	0.58	9300	−2570	9700	≥5	...	6
16A	SE	143	0.45	7300	+3500	8100	≥5	1.3	6
21A	NE	134	0.42	6800	−6530	9400	≥4	2.0	5, 6
21B	NE	144	0.46	7300	−6070	9500	≥3	...	5, 6
21C	NE	154	0.49	7800	−5550	9600	≥5	1.4	5, 6
21D	NE	171	0.54	8700	−4950	10000	≥5	2.2	5, 6
24	SW	222	0.70	11300	+3050	11700	≥3	3.3	6
24A	SW	227	0.72	11600	+2890	12000	≥2	2.5	6
25	SW	204	0.65	10400	+2220	10600	≥3	3.8	6
26	SW	196	0.62	10000	+3420	10600	≥6	4.5	6
60	JET	174	0.55	8900	−3800	9700	...	0.7	5, 6
61	JET	163	0.52	8300	−3780	9100	≥5	3.6	5, 6
62	JET	151	0.48	7700	−4240	8800	...	0.8	5, 6
63	JET	146	0.46	7400	−3960	8400	...	1.0	5, 6
65	JET	173	0.55	8800	−3140	9300	...	0.6	5, 6
66	JET	175	0.55	8900	−3370	9500	...	1.5	5, 6
66A	JET	179	0.57	9100	−2000 to −4000	∼9600	...	...	5, 6

NOTE.—Table 2 is also available in machine-readable form in the electronic edition of the *Astrophysical Journal*.

[a] Estimated 1996.7 radial distance from α[J2000] = 23^{h}23^{m}27^s.7, δ[J2000] = 58°48′47″.

[b] Implied average proper motion since A.D. 1680; $\langle\mu\rangle = R/316$ yr.

[c] Transverse velocities calculated assuming $d = 3.4$ kpc.

[d] In units of 10^{-16} erg cm^{-2} s^{-1} for epoch 1996–1998.

REFERENCES.—(1) Fesen, Becker, & Blair 1987; (2) Fesen, Becker, & Goodrich 1988; (3) van den Bergh & Kamper 1983; (4) Fesen & Becker 1991; (5) Fesen & Gunderson 1996; (6) this paper.

ejection velocity of around 10,000 km s^{-1} for almost all the four dozen [N II] emission knots detected.

A similar plot but now for FMKs and MEKs is shown in Figure 9*b*. Again, the solid circle indicates an average expansion velocity of 10,000 km s^{-1}. Here one sees no FMK or MEK preference for a specific expansion velocity. However, as in the case of the NKs, the smallest displacements are seen in the southeast, while the southwest shows the largest. A comparison of NKs versus FMKs + MEKs is shown in Figure 9*c*. This figure shows three important points. First, there is good agreement in the azimuthal location of the slower NKs and FMKs in the southeast. Second, in the southeast NKs lie always farther out than the FMKs for a given position angle. Third, the most distant, highest-

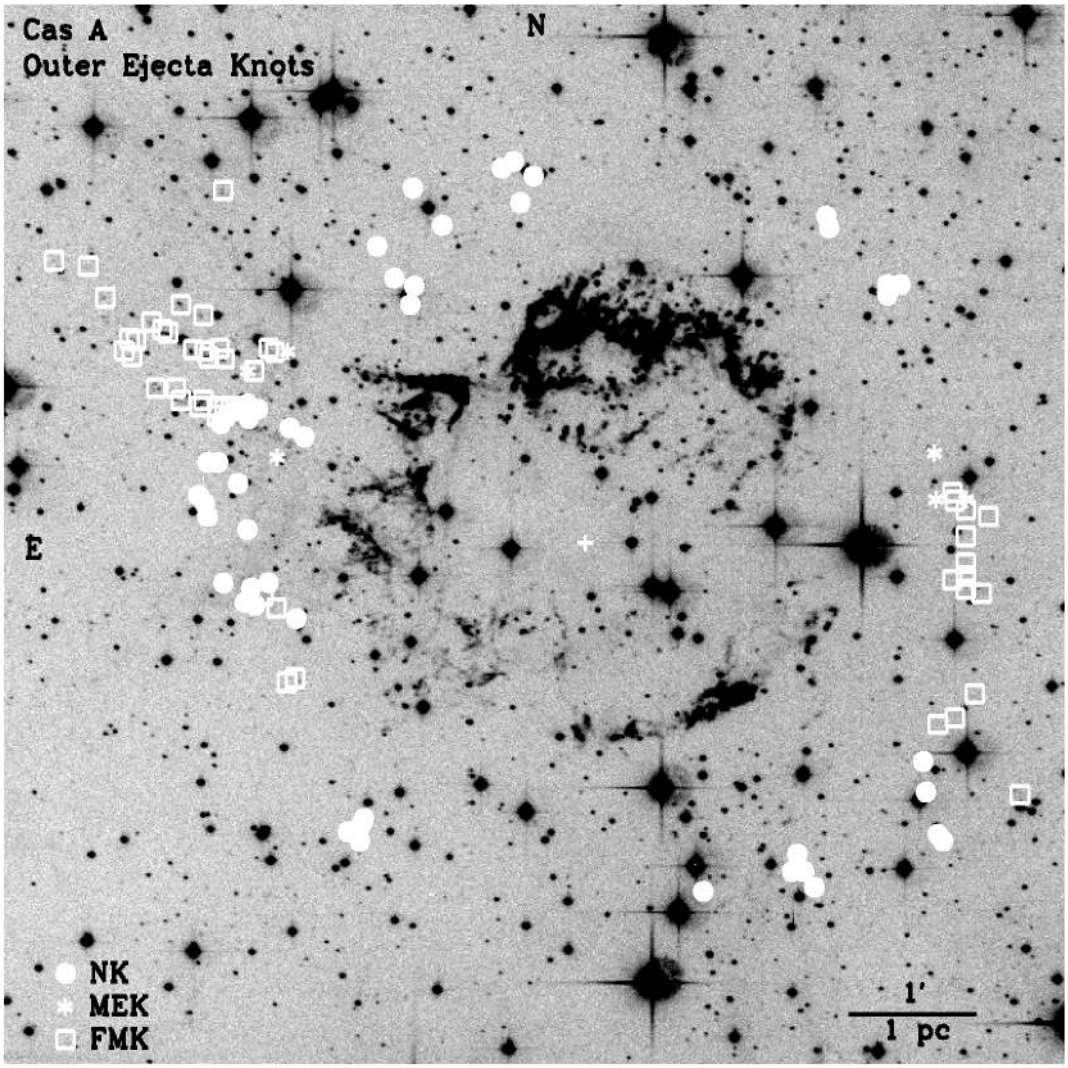

FIG. 5.—Relative locations of various outer ejecta knot types. Image is the same 1992 [S II] $\lambda\lambda$6716,6731 image of Cas A shown in Fig. 1. Knot symbol legend is shown at lower left. A small but representative number of jet FMKs (Fesen & Gunderson 1996) are included to better portray the remnant's outer ejecta distribution. The central white cross indicates location of the van den Bergh & Kamper (1985) estimated center of expansion.

velocity NKs in the southwest lie adjacent to the most distant FMKs.

As noted above and shown in Figures 9*b* and 9*c*, the highest velocity FMKs discovered in our optical survey possess space velocities in excess of 10,000 km s^{-1} and lie along the western and southwestern outskirts of the remnant. However, the remnant's overall highest-velocity ejecta lie in its northeast jet of knots. To examine all outer knots together in projected angular and azimuthal context, we show in Figure 9*d* all 75 outlying knots surveyed here together with the 86 jet FMKs studied by FG96. Once again the solid circle represents a 10,000 km s^{-1} expansion velocity, while the broken circle indicates a 6000 km s^{-1} expansion velocity, approximately equal to that of the main optical shell.

This figure reveals several new things. First, outlying FMK-type ejecta knots are found only along the eastern and western limbs. Second, the remnant's fastest western NKs and FMKs are located nearly 180° away from the remnant's high-velocity, northeastern jet. Third, the apparent NNW and SSE gaps seen in the NK distribution lie roughly orthogonal to this NE and SW alignment of highest-velocity FMKs. Possible interpretations of these features are discussed below.

4. DISCUSSION

Combined with previous studies, there are now some 75 optical knots known outside the remnant's main shell excluding the $\simeq$100 FMKs in the northeast jet. Although much fainter than main shell ejecta, the number and broad azimuthal distribution of these new outlying debris indicate a more significant population of $v_{\rm space} \geq 7000$ km s^{-1} ejecta than previously realized. In addition, many of these knots exhibit distinct chemical compositions not seen elsewhere in the remnant. By virtue of their expansion velocity alone (about twice that of the main shell) this material constitutes an important element of Cas A's total kinetic energy and thus offers insights into the expansion dynamics of this high-mass, core-collapse supernova.

The faintness of these optical knots largely explains why they went undetected in the many previous studies of Cas A. While the brightest NK-type knot, NK 15, was noticed as early as 1951 (Kamper & van den Bergh 1976), it was understandably interpreted as a [S II] emitting FMK

TABLE 3

OUTLYING, HIGH-VELOCITY S AND O EMISSION KNOTS (FMKs)

Knot ID	Limb Area	R[a] (arcsec)	V_T[b] (km s^{-1})	V_R (km s^{-1})	$V_{\rm Space}$ (km s^{-1})	[O III] λ5007	[O I] λ6300	[O II] λ7325	[S II] λ6725	λ6716/λ6731	N_e[c] (cm^{-3})
16	SE	153	7800	−475	7800	6.8	5.8	20.0	6.4	0.58	5000
17	SE	160	8200	−310	8200	...	1.3	7.7	...	...	...
17A	E	147	7500	+1020	7600	...	1.2	3.5	...	...	...
17B	E	152	7800	∼0?	≥7800	...	...	...	...	...	...
19A	W	187	9500	−830	9500	...	...	...	1.0	∼0.7	∼2000
19B	W	188	9600	−550	9600	...	...	...	1.4	0.62	4000
19C	W	187	9500	+460	9500	...	...	...	0.5	∼0.6	∼4000
19D	W	188	9600	+5500	11100	...	...	0.4	0.8	∼0.5	∼10000
19E	W	189	9600	+1330	9700	...	...	...	0.5	∼0.7	∼2000
19F	W	200	10200	+4550	11200	...	...	1.4	2.7	0.55	6500
19G	W	196	10000	−550	10000	...	...	...	0.7	∼0.6	∼4000
19H	W	202	10300	−830	10300	...	...	...	2.8	1.37	50
19I	W	181	9200	−1010	9300	...	...	4.5	2.6	0.65	3000
19J	W	184	9400	...	≥9400	...	...	...	...	...	...
19K	W	182	9300	+5190	10700	...	...	4.3	3.2	0.85	1100
19M.....	SW	201	10300	+3700	11000	...	...	...	2.8	0.75	1700
22	SW	194	9900	+3520	10500	...	...	...	1.6	∼0.6	∼4000
23	SW	243	12400	+2070	12600	...	...	...	5.0	0.80	1500
27	NE	245	12500	−270	12500	...	...	...	6.3	0.65	3000

NOTES.—Observed line fluxes are in units of 10^{-16} erg cm^{-2} s^{-1}. Table 3 is also available in machine-readable form in the electronic edition of the *Astrophysical Journal*.

[a] Estimated 1996.7 radial distance from $\alpha[J2000] = 23^{\rm h}23^{\rm m}27\overset{\rm s}{.}7$, $\delta[J2000] = 58°48'47''$.

[b] Implied average transverse velocities calculated assuming $d = 3.4$ kpc and a 316 yr expansion age.

[c] Electron densities derived from [S II] 6716/6731 ratio assuming $T = 10^4$ K.

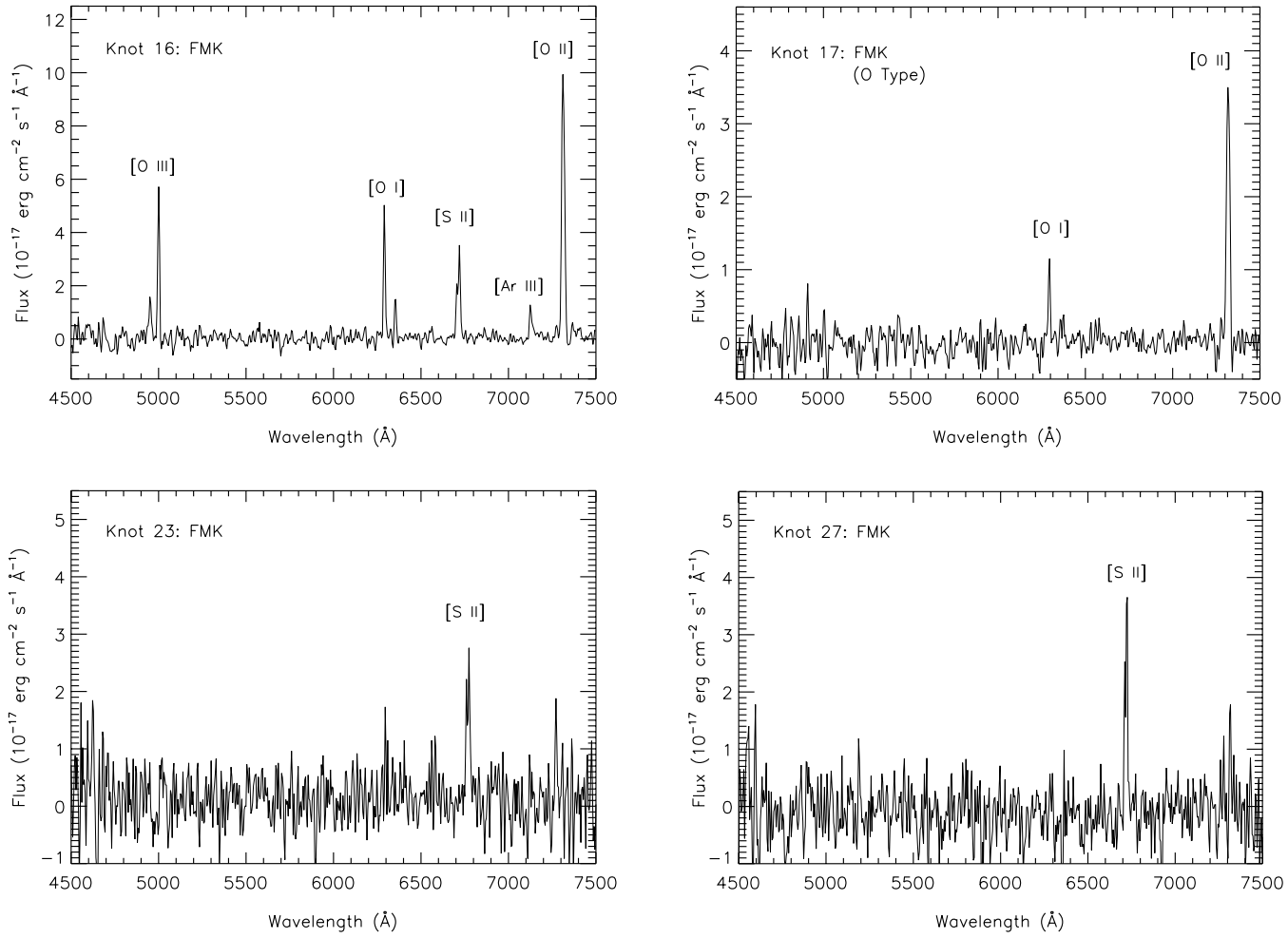

FIG. 6.—Spectra of four metal-rich, outlying ejecta knots (FMKs) in Cas A

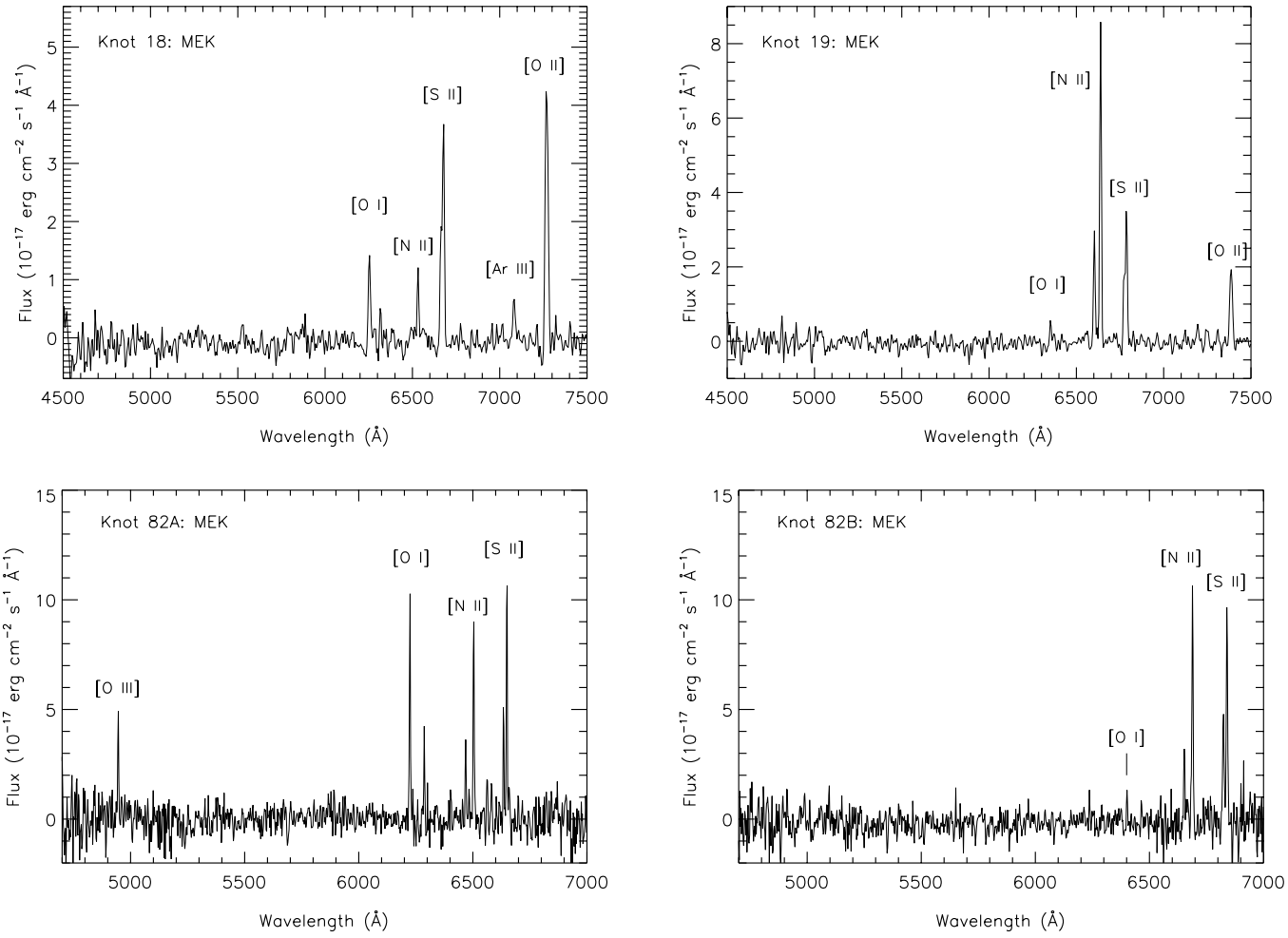

FIG. 7.—Spectra of four high-velocity, "mixed emission knots" (MEKs) in Cas A

knot, rather than a bright member of a larger population of N-rich outer ejecta. Even if its true nature had been realized sooner, the majority of outer NK/FMK knots would not have been detected on broadband photographic plates even with exposures of several hours duration using 4–5 m class telescopes. Subsequent examinations of 1951–1985 archival Palomar 5 m plates do reveal a few weak detections of a couple of the brighter outer knots (Kamper & van den Bergh 1991), but these are exceptions. Also, the first deep CCD imaging of the remnant's outskirts concentrated on imaging using Hα filters, thereby missing any new FMK-type knots (FBB87; FBG88).

The surprising success of our modest survey suggests additional outer knots are likely to exist. The radial velocity range to be searched is large (± 7000 km s^{-1}) with a variety of dominant knot emission lines possible ([N II] λλ6583,6548, [S II] λλ6716,6731, and [O I] λ6300). These factors combine to make the wavelength search region formidable ($\sim$6000–7000 Å) using conventional narrow passband filters. Our survey did not have sufficient filters to

TABLE 4

OUTLYING, HIGH-VELOCITY MIXED EMISSION KNOTS (MEKs)

Knot ID	Limb Area	R[a] (arcsec)	V_T[b] (km s^{-1})	V_R (km s^{-1})	$V_{\rm Space}$ (km s^{-1})	[O I] λ6300	[O II] λ7325	[S II] λ6725	[N II] λ6583	λ6716/λ6731	N_e[c] (cm^{-3})
18.....	W	175	8900	−2350	9200	1.9	8.7	7.0	1.2	0.51	11000
19.....	W	188	9600	+2400	9900	0.5	3.3	6.2	9.7	0.50	13000
20.....	W	171	8700	−920	8800	...	0.5	0.9	≃0.3	∼0.70	∼2000
82.....	JET	181	9200	+5100	10500	6.5	18.3	21.0	7.1	0.60	4000
82A.....	JET	151	7700	−3630	8500	5.3	16.5	7.9	5.2	0.49	16000
82B.....	JET	170	8700	+4830	10000	0.5	...	10.5	7.0	0.53	8200

NOTES.—Observed line fluxes are in units of 10^{-16} erg cm^{-2} s^{-1}. Table 4 is also available in machine-readable form in the electronic edition of the *Astrophysical Journal*.

[a] Estimated 1996.7 radial distance from $\alpha[J2000] = 23^{\rm h}23^{\rm m}27\overset{\rm s}{.}7$, $\delta[J2000] = 58°48'47''$.

[b] Implied average transverse velocities calculated assuming $d = 3.4$ kpc and a 316 yr expansion age.

[c] Electron densities derived from [S II] 6716/6731 ratio assuming $T = 10^4$ K.

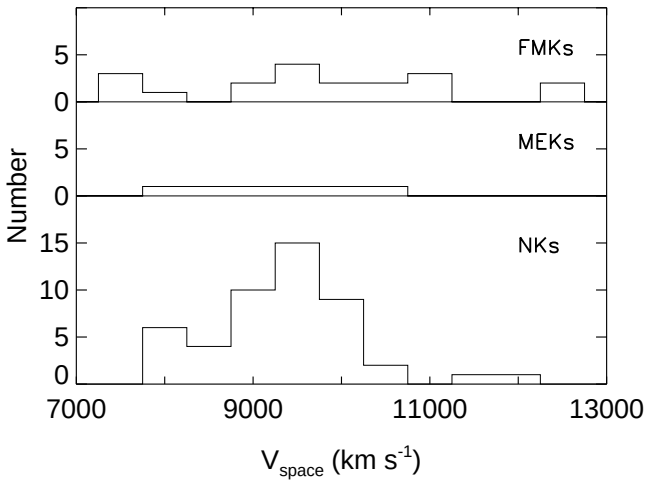

FIG. 8.—Histograms of inferred knot space velocities vs. knot population for Cas A's high-velocity, outer ejecta, binned by knot type.

conduct a complete search of this whole spectral range. Moreover, increased extinction toward Cas A's western limb (Troland, Crutcher, & Helies 1985; Bieging & Crutcher 1986; Keohane, Rudnick, & Anderson 1996; Schwarz et al. 1997) could easily hide a larger population of faint outer debris in this direction.

Nonetheless, the 75 knots discussed below, together with the 80+ knots previously studied in the NE jet region, provide a more complete look at the structure and kinematics of the remnant's outer debris than previously possible.

4.1. *Knot Visibility Factors*

The 50 currently known NKs span a relatively wide range of radial velocities, namely, -6500 to $+5700$ km s^{-1}. For these to exhibit similar space velocities as shown in Figure 9*a* implies a significant range of locations out of the plane of the sky. For instance, Knots 21A–21D lie some 30°–44° off the plane moving toward us, and Knots 14 and 15 lie 34° and 28° off the sky plane moving away. Such large angles off the sky plane appear, however, to be the exception with the majority of detected nitrogen knots lying within $\pm 20°$ of the sky (see Fig. 11). Larger angles would project the knots against the main shell, but there are no reported detections of such high-velocity [N II] emitting main shell knots (Reed et al. 1995). Relatively small angles off the sky plane also seem to be the rule for the FMKs and probably for the MEKs as well, although there are too few to really determine their distribution. These results suggest that, as seen to hold true for main shell emission knots, a near tangent viewing angle is an important factor in producing knot visibility for outer ejecta knots of all types.

A near tangent viewing angle requirement for optical knot detection is also consistent with a lack of visible ejecta with unusually high radial velocities near Cas A's center. Although our images were inadequate to survey emission knots covering the full NK velocity range of $\pm 12{,}000$ km s^{-1}, it appears unlikely that relatively bright optical knots with $v \geq 8000$ km s^{-1} exist toward the remnant's center. Deep broadband *R* images which do detect the brighter NKs, show virtually no emission of any sort near the remnant's center ($\sim 30''$ radius). Also, our 6450 and 6510 Å images would have detected blueshifted [S II] emission having velocities $\simeq -9000$ to $-13{,}000$ km s^{-1} and our broad [S II] images were sensitive to redshifted [N II] λ6583,6548 emission out to $\sim +8000$ km s^{-1}. Finally, no extraordinarily high-velocity ejecta emission was seen in several exploratory, long-slit spectra taken across the remnant center.

Detection of NKs and FMKs in groups or small clusters in particular regions suggests that the presence of extended CSM and/or ISM of sufficient density is also required for creating strong optically emitting shocks in the ejecta. A relatively bright H II region sits off the remnant's eastern limb (Fig. 10; see also FG96 and Reynoso et al. 1997). High-speed knot passage through this H II region is the likely cause for the large number of optically visible NKs and FMKs in this area (Fig. 5). The relatively bright, FMK-rich jet region lies just northward and likewise may owe much of its optical visibility to strong interactions within and around the northern parts of this H II region. Much fainter patches of emission can be seen (in projection) outside Cas A's SW and NW limbs and these might play similar roles. However, a physical connection of these with the remnant is unclear, and no diffuse optical emission features are visible along much of the remnant's limb where optical knots are detected nonetheless.

4.2. *Location of Outer Optical Knots with Respect to Cas A's Radio and X-Ray Emission*

Though there have been recent Cas A radio versus X-ray emission comparisons (e.g., Keohane, Rudnick, & Anderson 1996; Koralesky et al. 1998), there are few optical versus radio or optical versus X-ray comparisons (Ryle, Elsmore, & Neville 1965; Hogg et al. 1969; Fabian et al. 1980; Dickel et al. 1982) and only one done in the last decade (Reynoso et al. 1997). This has made it difficult to examine positional coincidences between these outer optical knots and Cas A's outermost radio and X-ray emissions. This issue is particularly relevant for determining whether these knots lie ahead of or behind Cas A's outer blast wave.

Figure 5 shows that all 75 ejecta knots lie well outside of the remnant's bright optical shell. In order to see where these knots lie relative to the remnant's outermost radio and X-ray emissions, we present two sets of radio/X-ray versus optical knot comparisons. Figures 12*a* and 12*b* show VLA 20 cm continuum and *Chandra* ACIS-S X-ray emission contours, respectively, overlaid onto the same 1992 [S II] optical image shown in Figures 1 and 5. The seemingly "empty" regions inside the innermost contours on these figures denote areas of particularly bright radio or X-ray emission. This presentation of the data allows one to see how the bright radio and X-ray regions match up with bright optical areas with less inner contour confusion. The outermost radio emission contour represents a flux level $\simeq 0.1$ mJy, comparable to that shown by Reynoso et al. (1997). Although there is a mismatch of several years due to the different epochs at which these three data sets were obtained (optical: 1992, VLA: 1994/1995; X-ray: 1999), nonetheless the figures illustrate a fact that has been known for sometime, namely, that considerable radio and X-ray emissions lie well outside the remnant's bright optical emission shell.

Where do the outlying optical knots lie in relation to these outer radio and X-ray emissions? Figures 13*a* and 13*b* show these same VLA radio and *Chandra* X-ray image data versus the positions of the 75 outer optical knots as shown

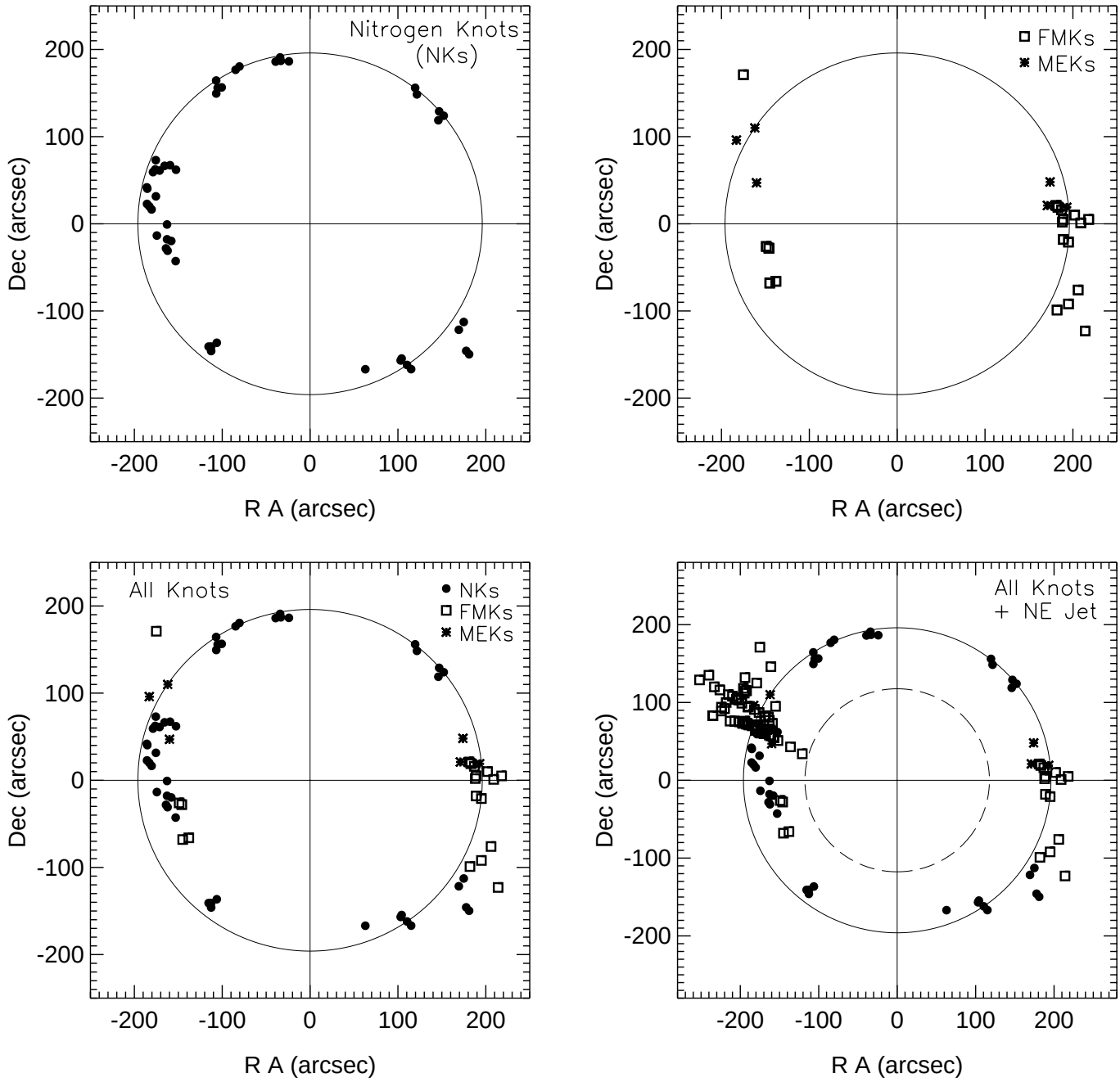

FIG. 9.—Projected angular displacements from Cas A's nominal expansion center for all detected high-velocity, outlying knots as a function of knot types. Symbols used are the same as in Fig. 5. Panels (*a*)–(*c*) show NKs, FMKs + MEKs, and NKs + FMKs + MEKs, respectively. Solid circles mark the angular displacement for $V_{exp} = 10{,}000$ km s^{-1}. Panel d shows plot of locations of all knots plus 80+ knots in the remnant's NE jet (Fesen & Gunderson 1996). The solid circle represents $V_{exp} = 10{,}000$ km s^{-1}, whereas the inner dotted circle represents $V_{exp} = 6000$ km s^{-1}, roughly equivalent to the expansion velocity of the remnant's bright optical shell.

in Figure 5. Even ignoring possible knot radial velocities, all outlying optical knots along the western limb and many of the eastern ones lie outside of the radio emission edge (Fig. 13*a*). A similar situation is found for the remnant's X-ray emission (Fig. 13*b*). If the line of thin, wispy X-ray emission filaments at a radial distance $\sim 160''$ marks the location of the remnant's outermost shock front (Vink et al. 1998; Gotthelf et al. 1999; Hughes et al. 2000), then all of the western knots lie out beyond Cas A's main blast wave. If one adds in the knots' radial velocities (Tables 2–4) to these projected positions, their projected radial positions would be even farther out. This means that most, if not all, outlying optical knots are moving out ahead of the shock front into unshocked CSM or ISM in a fashion like that discussed by Hamilton (1985).

4.3. *Radio and X-Ray Features Associated with Outlying Optical Emission*

There are few if any confirmed instances of spatial coincidences between individual optical and radio emission knots in Cas A's bright main shell (Anderson et al. 1994). The same appears true in the X-rays as well (Fabian et al. 1980). However, the base of the NE jet exhibits considerable radio and X-ray emission in rough agreement with the loca-

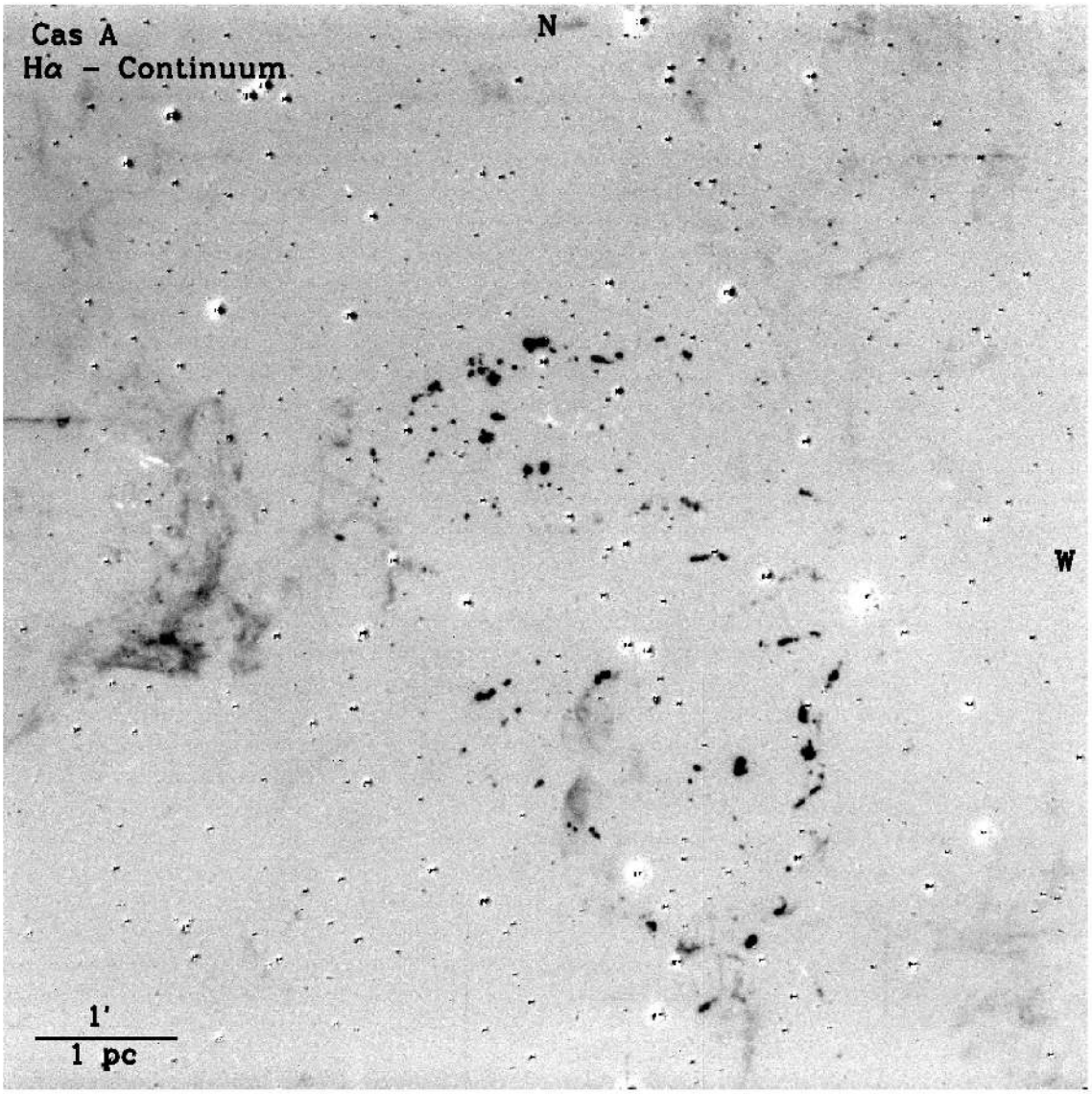

FIG. 10.—A 1998 Hα minus continuum (6510 ± 15 Å) image of the Cas A remnant and projected local vicinity. Numerous bright QSFs, several small diffuse clumps of emission, and larger extended diffuse emission features are visible.

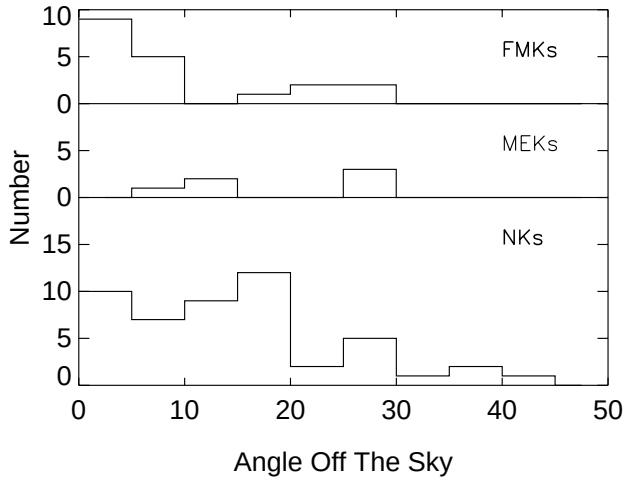

FIG. 11.—Histogram of knot angular displacement (absolute degrees) off the plane of the sky vs. knot population for each knot type.

tions of the jet's lower velocity FMKs. In addition, Braun, Gull, & Perley (1987) found several bow-shaped radio emission features along Cas A's limb, one of which (their Feature "H") appeared to be associated with an outlying optical QSF (R36; van den Bergh & Kamper 1985) along the SW rim (see also Bell, Gull, & Kenderdine 1975).

We can now see additional optical/radio/X-ray emission coincidences, specifically along the southeastern limb at the locations of some outlying optical knots. As shown in Figures 12 and 13, there is enhanced radio and X-ray emission near the locations of Knots 4 through 6A, and Knots 16 through 17. Interestingly, Reynoso et al. (1997) found two small H I absorption clouds in this region (their Features 14 and 15) which may be related to the observed optical knot emissions. The best spatial coincidences between our optical knots and the 20 cm and H I absorption involve FMK Knots 16, 17, 17A, and 17B. These knots also lie at the outer tips of a bright clump of X-ray emission (Figs. 12*b* and 13*b*).

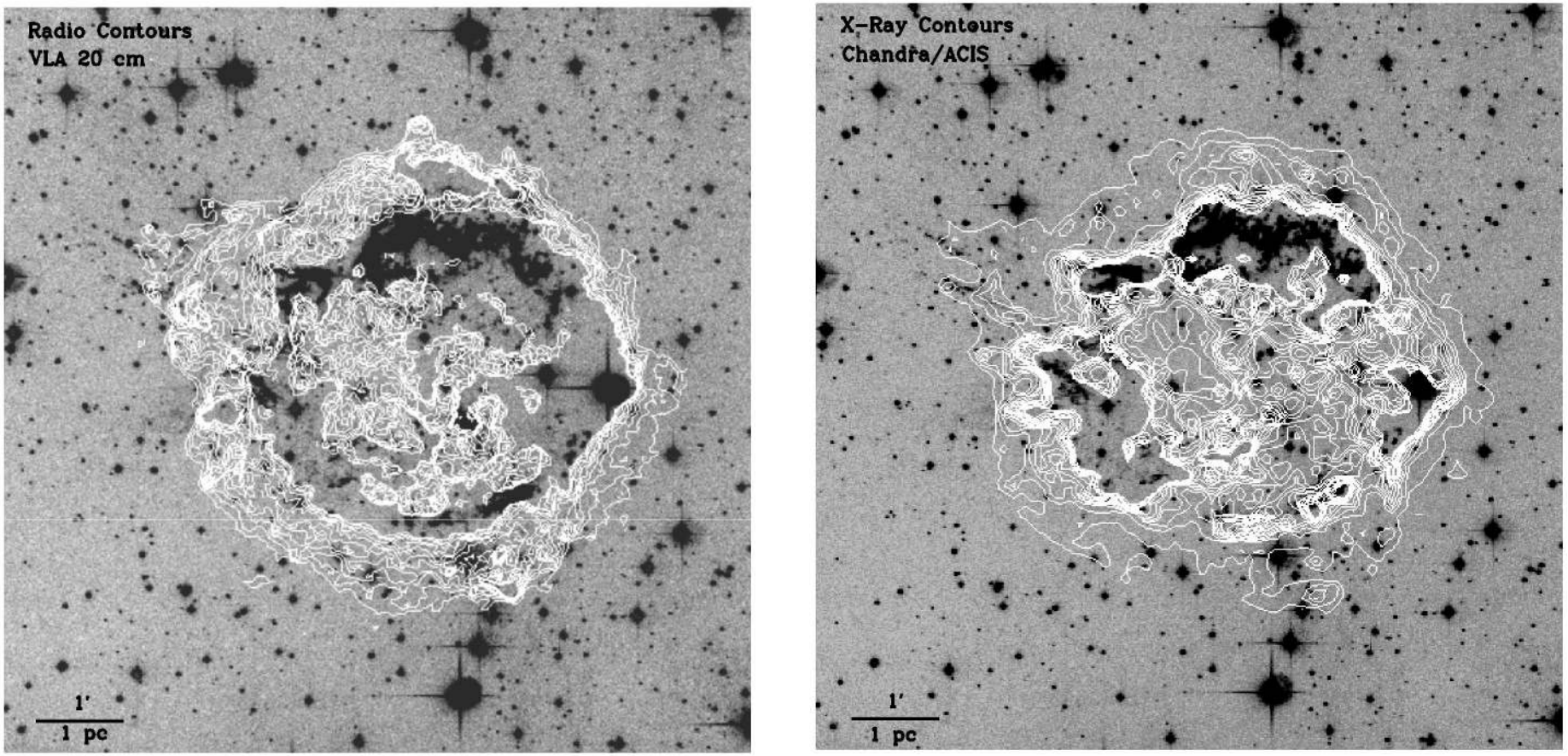

FIG. 12.—(*a*) Flux contours of VLA 20 cm continuum map of Cas A (epoch 1994/1995; Anderson & Rudnick 1995, 1996) are shown (*white lines*) overlaid onto a 1992 optical [S II] image (Fesen & Gunderson 1996). (*b*) Flux contours of the *Chandra* ACIS-S image of Cas A (0.6–7.5 keV; Hughes et al. 2000) are shown (*white lines*) overlaid onto a 1992 optical [S II] image (Fesen & Gunderson 1996).

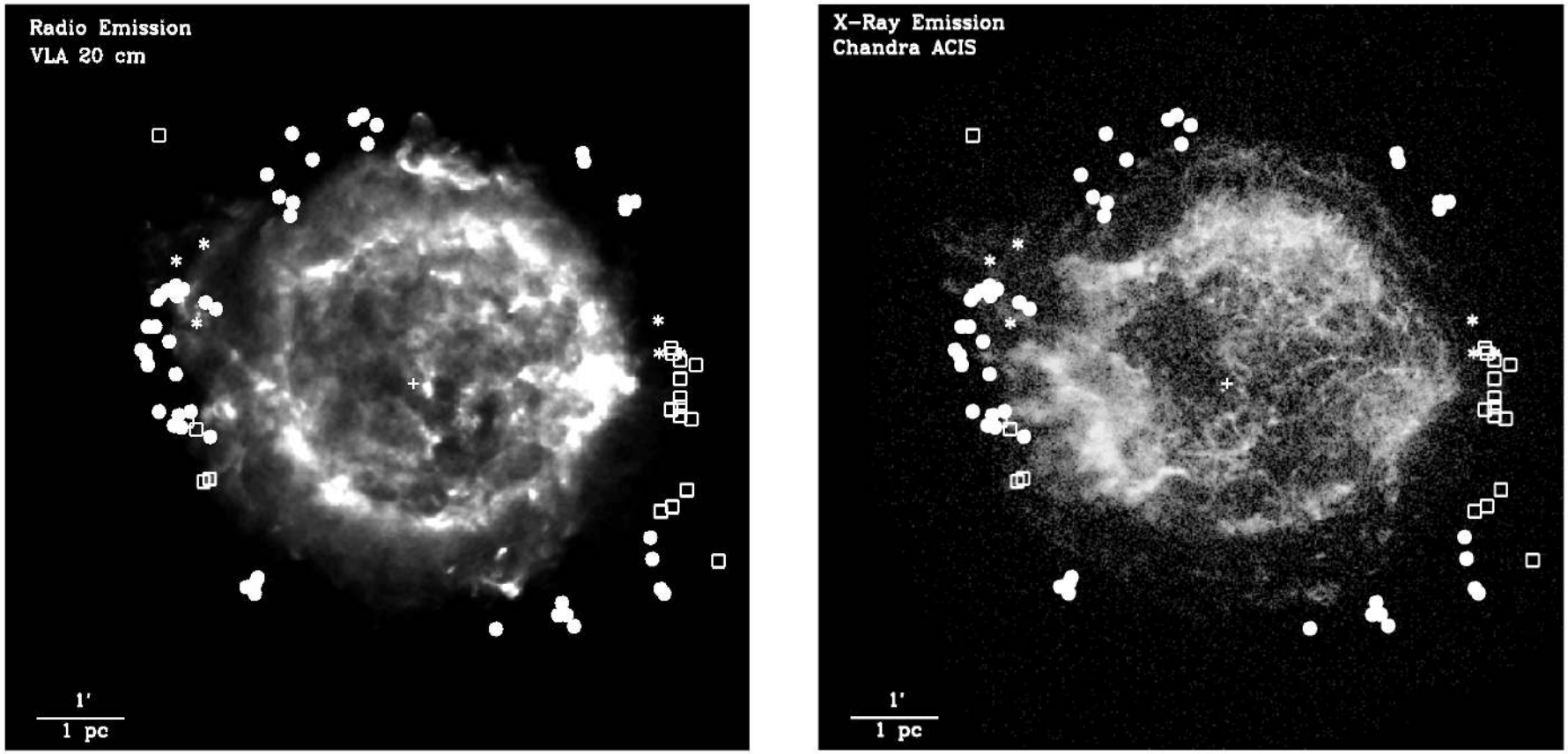

FIG. 13.—(*a*) VLA 20 cm radio continuum image of Cas A (1994/1995 epoch; Anderson & Rudnick 1995, 1996) with locations of outlying optical knots indicated. Knot symbols are the same as in Fig. 5. The remnant's expansion center is indicated by the white cross. (*b*) *Chandra* ACIS-S (0.6–7.5 keV; Hughes et al. 2000) X-ray image of Cas A is shown with locations of outlying optical knots indicated. Knot symbols are the same as in Fig. 5. The remnant's center of expansion is indicated by white cross.

There is also an interesting optical/radio emission coincidence along the remnant's northern edge. It involves a peculiar radio emission arc with a brightness comparable to that of the main shell lying some 30″ north of Cas A's bright radio ring. This filamentary arc is the largest and brightest extended emission outside the main shell and is readily apparent in maps of the remnant (Bell, Gull, & Kenderdine 1975; Tuffs 1986; Braun, Gull, & Perley 1987). A portion of the VLA 20 cm image showing this filament is presented in the upper right-hand panel of Figure 14. Although little coincident X-ray emission is seen here (Koralesky et al. 1998), the feature does have a strong infrared counterpart. ISOCAM aboard the *Infrared Space Observatory* detected a featureless infrared continuum at this location which has been attributed to CSM or ISM silicate dust at 105 K associated with a local cloud which has undergone shock heating by the Cas A blast wave (Douvion et al. 1999). Its projected location outside the main shell but behind the outer, X-ray blast wave emission is consistent with this picture.

We have also discovered some faint optical emission apparently associated with this radio filament. A deep *R*-band image of this region (Fig. 14, *upper left panel*) reveals an exceedingly faint patch of diffuse optical emission whose position and morphology roughly matches that of the radio filament (Fig. 14, *lower left panel*) and infrared (Lagage et al. 1996). While most visible in the *R*-band image, it could be faintly seen also in narrow and broad [S II] images.

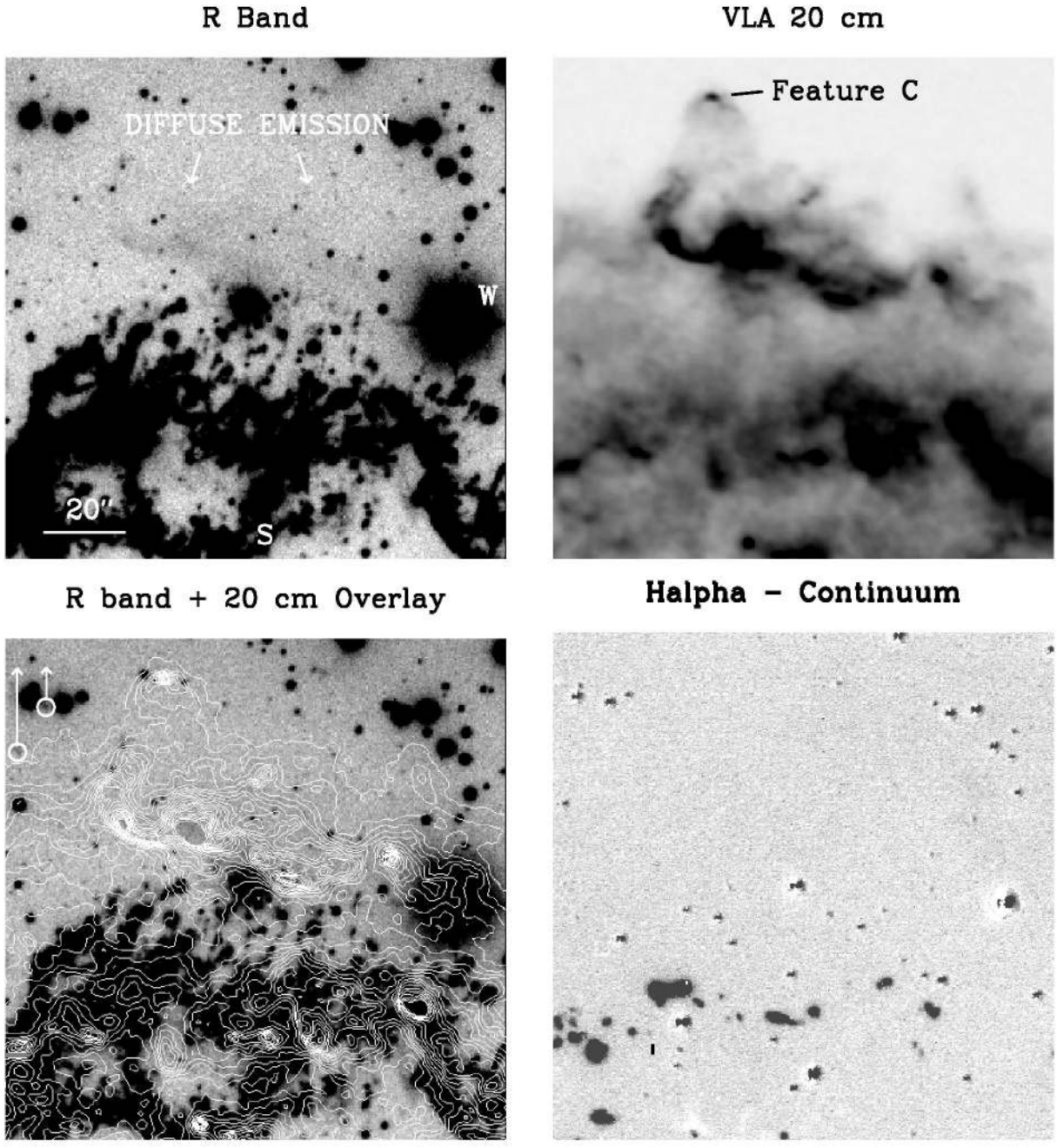

FIG. 14.—Optical and 20 cm VLA radio emission map comparisons for limb region just north of main shell. Scale in top left panel applies to all panels.

However, because this diffuse emission is not seen in deep Hα images (Fig. 14, *lower right panel*), its emission is not that of an H II region.

This diffuse optical emission may be a reflection nebula associated with the IR detected CSM/ISM cloud whose dust is reflecting the bright [S II], [O I], and [O II] line emissions of Cas A's bright northern optical ejecta. This would explain why it is best seen in the broad passband *R* image. The combined [S II], [O I], and [O II] line emissions from Cas A's bright ejecta could make the reflecting nebula detectable. A dusty cloud in this location might also partially explain the apparent lack of detected optical knots in this northern limb area (see Fig. 5). A deep optical spectrum could test this hypothesis.

4.4. *Outer Radio Bow Shocks and High-Velocity, Optical Knots*

A neighboring, compact radio feature may be related to some of our newly discovered high-velocity, outlying optical knots. Just north of the bright radio filament discussed above, Braun, Gull, & Perley (1987) argued that a small bow-shaped feature seen there (their Feature "C"), like several others around the edges of the remnant, was formed by tenuous clumps of intermediate velocity (4700–6500 km s^{-1}) debris puncturing a decelerated shell with $v = 2300$–3900 km s^{-1} created by formerly higher speed diffuse ejecta.

Radio Feature "C" can be seen in the 20 cm VLA image shown in Figure 14 (*upper right panel*). It appears as a faint, bow-shaped cone of outlying emission with a bright knot at its northern apex. A Mach number of 2.3 was suggested based on a opening half-angle of 26° for the faint trailing emission (Braun et al. 1987). Anderson & Rudnick (1995) noted that such a low Mach value is inconsistent with passage through unshocked circumstellar medium, thereby suggesting formation within a high-velocity, post-blastwave fluid as in the Braun et al. (1987) scenario. They estimated a proper motion velocity for this feature of 4300 km s^{-1}, which in turn suggested a post-blastwave fluid velocity of ~ 1670 km s^{-1} for $\gamma = 5/3$.

There are several problems, however, with a bow-shock scenario for this radio feature. First, the physical meaning of its radio-derived proper motion velocity of 4300 km s^{-1} is unclear since radio derived expansion ages for this $\simeq 320$ yr old remnant span 550 to 900 yr for outer and inner features, respectively (Anderson & Rudnick 1995). Second, much of Feature C's emission structure lies out beyond the remnant's blast wave as seen in the most recent X-ray maps of the remnant (Gotthelf et al. 1999; Hughes et al. 2000). This makes passage of ejecta through a "post-blastwave fluid" problematic. If there were a decelerated shell of diffuse ejecta farther out and ahead of Feature C, there is no hint of it in radio, X-ray, optical, or infrared emission maps. Third, the northern tip of Feature C lies at a greater radial distance ($\simeq 180''$) than any "intermediate velocity" ejecta could possibly reach at the present time. In the lower left panel of Figure 14 we have marked the observed positions of NKs 15 and 15A (*small white circles*). These optical knots have radial distances from the Kamper & van den Bergh (1976) center of expansion of 168″ and 178″, implying transverse velocities of 8600 and 9100 km s^{-1}, respectively. The fact that these high-velocity ejecta appear *behind* in projection the position of the radio bow-shock means that Feature C must have a space velocity exceeding 9000 km s^{-1}. This inconsistency with the radio derived 4300 km s^{-1} proper motion grows larger if Feature C has any significant motion out of the sky plane (e.g., the nearby knot NK 15 has a radial velocity of $+4500$ km s^{-1}).

Strong decelerations of northern limb NKs could, in principle, help explain their discordant radial placements relative to Feature C. However, proper motion data suggest that NK-type knots in this northern region have experienced very little deceleration (see Fig. 9*a*). For example, Knot NK 15 has a proper motion of $0''.525 \pm 0''.005$ yr^{-1} (van den Bergh & Kamper 1983), implying an explosion date of A.D. 1677 ± 4 and thus an average deceleration of 2% or less if A.D. 1680 is taken as the date of the Cas A SN.

An alternative model is that the bow-shock feature is due to a small cluster of NK-type knots passing through the northern portion of the diffuse local CSM/ISM cloud discussed above. This cluster could produce a shock wave structure that could resemble a low Mach cone off a single high-speed knot. There are several points favoring this interpretation. First, an association of outlying optical knots with this bow shock is suggested by the similarity of radial positions from the remnant's center. In Figure 14 (*lower left panel*) we show the projected space velocity displacements for NKs 15 and 15A by the white arrows on the open circles. One sees that these NKs would have displaced radial positions equal to that for the bright apex of the radio bow-shock feature assuming its motion is largely in the sky plane. Second, an extension of this CSM/ISM cloud farther to the north than depicted by its radio or infrared emission is suggested by the absence of stars in this region (Figs. 5 and 14). Last, examination of the VLA radio image indicates the presence of a fainter, companion knot $\approx 5''$ off to the southwest of the bright apex knot. A small grouping of small ejecta knots would be consistent with that found elsewhere in the remnant (see § 3.1).

In summary we propose: (1) The diffuse radio, infrared and now optical emission seen along the north limb region originates in an CSM/ISM cloud located just outside of Cas A's main shell. (2) Clumps of high-velocity ejecta, like that seen in the optical elsewhere in the remnant, have partially transversed this cloud and are currently located along its northern edge. (3) The collective effects of several high-speed knots through this cloud could produce the bow-shock–like structure observed in the radio.

4.5. *Outer Ejecta Chemical Compositions*

Spectra for 68 of the 75 outer knots listed in Tables 2–4 show that these outer knots possess distinct chemical makeups. A detailed quantitative analysis of the chemical composition of these outer knots using customized, metal-rich shock models is beyond the scope of this paper. However, several qualitative statements can be made from the available data using published shock models.

Whereas no high-velocity, main shell knots have been observed to show a spectrum dominated by nitrogen line emission, there are now four dozen knots (NKs) located outside the shell that do. As noted in § 3.1, Hα emission it is usually too weak to detect or measure accurately in these knots. In the few cases where Hα is seen, it is usually considerably weaker than the weak [N II] λ6548 line. From data on 10 NKs, FBG88 estimated N/H levels at least 10 times solar. Our much larger sample suggests that such large N/H abundances ratios are the rule rather than the exception.

The presence of Hα emission in a few NKs with strengths like that of the pre-SN QSF mass-loss material has been cited as evidence for photospheric hydrogen at the moment the progenitor star exploded (FBG88). If true, this would set important constraints on the progenitor's mass-loss development phase. Also, subsequent detections of N and H lines in mixed jet knots was given as supporting evidence that a H-rich outer layer might have permitted the Cas A SN to briefly exhibit a Type II spectrum near maximum light (FB91; FG96). However, from our sample of 44 NK spectra, we find QSF-like Hα/[N II] line strengths in only three knots, namely NKs 1–3 in the SW region. In addition, none of the three new western or the two jet MEKs (Knots 82a,b) show any detectable Hα emission (e.g., I([N II]λ6583)/I(Hα) ≥ 10 for Knot 19). Since significant mass accretion of circumstellar or interstellar material onto these high-speed knots seems unlikely, the H + N rich photospheric layers must either have been of very low mass or did not form into many observable optical knots.

Regarding outlying FMKs, there appears to be significant chemical differences between them and the FMKs in Cas A's bright main shell. Specifically, we find evidence for a correlation of S/O abundance with expansion velocity. The [O III] λλ4959,5007 and [O II] λλ7319,7330 emissions, which are among the strongest lines seen in the spectra of main shell FMKs, appear strong only in the slowest outlying FMKs (Knots 16, 19I, and 19K; $v_{\rm space} \leq 10{,}000$ km s^{-1}). Also, [S II] λλ6716,6731 is rarely dominant in main shell knots, with just 8% of knots exhibiting a spectrum showing only [S II] emission present (Reed et al. 1995). However, [S II] dominant spectra appear common in outer FMK ejecta, with $O^0 \rightarrow O^{+2}$ line emissions either weak or below our detection limits when $v_{\rm space} \geq 11{,}000$ km s^{-1}.

A correlation of increasing [S II] dominated emission knots with high space velocity was also observed in the jet's FMKs (van den Bergh 1971; Fesen & Gunderson 1996) where paradoxically the high ionization lines of [O III] λλ4959,5007 virtually disappear above a knot velocity of 10,000 km s^{-1}. From just the small number of FMKs examined here, a [S II] versus expansion velocity correlation for outer FMKs is uncertain. However, when combined with the 80+ knots studied in the jet (FG96), the effect gains credibility.

Decreasing [O II]/[S II] with velocity is unlikely to be due to decreasing knot density and hence less collisional de-excitation of the [S II] lines as proposed by Reed et al. (1995) for main shell FMKs. They argued that systematically lower electron densities (and hence lower gas pressures) along with increasing expansion velocity could result in less [S II] collisional de-excitation and hence stronger [S II] λλ6716,6731 emission relative to less de-excited lines such as those of [O II] λ7325. Despite other evidence supporting abundance changes with ejection velocity, collisional de-excitation of the [S II] lines could not be ruled out in the jet FMKs where $N_e \leq 2 \times 10^3$ cm^{-3} (FG96).

From our estimates of the electron density sensitive [S II] λ6716/λ6731 line ratio, we have determined electron density values for 15 of the 19 new FMKs (Table 3). If we exclude the suspiciously low value for knot 19H, then $N_e \simeq 1.5$–10×10^3 cm^{-3} (I[6716]/I[6731] = 0.5–0.8) with an average value around 4000 cm^{-3} for Knots with $v_{\rm space} \geq 10{,}000$ km s^{-1}. Such densities are similar to those measured for FMKs located in the remnant's bright optical shell and generally are higher than those seen in the jet. Thus, the new FMKs show higher densities than those found in jet FMKs, yet exhibit similarly [S II] dominated spectra for the fastest knots. This means that increased S/O abundance ratios and not density differences account for the observed [S II] dominance in the highest velocity FMKs.

Last, there is the question about the true nature of the hybrid MEK-type knots. Without higher spatial resolution, it is unclear if these knots represent microscopically mixed N + O, S, Ar ejecta or are simply small clusters of chemically distinct debris knots. The bright western MEK Knot 19 is just barely resolved in subarcsec seeing, suggestive of a largely singular, thoroughly mixed NK/FMK knot. On the other hand, the extended appearances of some MEKs like the original Knot 82 in the jet (see FB91) and Knot 20 along the western limb (Fig. 2*j*) suggest we might be observing merely closely spaced NK and FMK knots. Although identical radial velocities for NK and FMK-type emission lines do support the mixed knot model, it does not prove it. If neighboring NK/FMK cluster knots were separated by 0.″5 at a radial distance of 180″, emission line radial velocities would differ by less than 0.3%. This would produce an easily unnoticed ≤25 km s^{-1} velocity difference in low-dispersion spectra.

4.6. *Asymmetrical Expansion and Turbulent Mixing*

It has long been suspected that the Cas A supernova may have undergone an asymmetrical expansion which lead to substantial mixing of the emerging ejecta. One obvious feature suggesting this is the "jet" of FMK-type ejecta off the remnant's northeastern limb. More than 30 years ago, Minkowski (1968) puzzled over its nature which he could detect out to a radial distance nearly twice that of the main shell. Derived proper motions combined with radial velocity data led van den Bergh & Dodd (1970) to conclude that different fragments must have left the Cas A supernova with widely differing space velocities. Later, due to the dominance of [S II] emission in a majority of jet knots, van den Bergh & Kamper (1983) speculated that S-rich knots, and not the expected overlying O-rich material, had been somehow ejected with the highest velocities in this area. More recently, Fesen & Gunderson (1996) found further indications for higher sulfur and argon abundances with increased jet ejecta velocity. They also detected jet emission knots out to a radial distance of ≃290″ implying a velocity of 15,000 km s^{-1}. This is 2.5 times the expansion velocity observed in the main shell and is strong evidence that the Cas A supernova did not experience a uniform spherical expansion.

Our survey of the remnant's outermost ejecta provides further clarification on how the Cas A supernova exploded. After allowing for knot decelerations along the eastern limb, the similarities of space velocities for the outer N-rich knots point to a nearly uniform ejection velocity of around 10,000 km s^{-1}. This suggests a fairly smooth, spherical expansion of the star's outermost layers. The fact that we see this velocity pattern in knots moving up to 30° into and out of the plane of the sky (§ 4.1) means that this expansion uniformity applies to at least one-third of the remnant.

A near spherical expansion, however, was apparently not shared by the progenitor's inner S and Ar-rich material. First, there is the northeast jet of ejecta which extends out to 15,000 km s^{-1}. Discovery of 7500–12,500 km s^{-1} velocity FMKs in the west, southwest, and southeast means that the jet's high-velocity FMKs can no longer be considered pecu-

liar. Second, the presence of both western and eastern FMK ejecta with space velocities above 11,000 km s^{-1} rich in the products of explosive O-burning indicates an asymmetrical expansion in more that one direction. Sulfur-rich material from the progenitor's innermost layers was ejected up through overlying layers at sufficient energies that their final velocities surpass even those of the usually fastest, less dense photospheric layers. What is unknown, however, is what process led to this asymmetrical expansion.

The presence of FMKs on opposite sides of Cas A raises the possibility of some sort of axisymmetric, bipolar expansion. The highest ejecta velocities ($\geq$12,000 km s^{-1}) lie in the northeastern jet (position angles $\sim$45°–70°) while the fastest western NKs and FMKs are found nearly 180° around (position angles $\sim$230°–260°; Fig. 9*d*). Although we found outlying O, S, Ar knots occupying a fairly broad azimuth distribution in the east and west, they subtend about the same $\sim$40° angular spread in both directions. Additional support of this picture comes from recent deep *Chandra* images of Cas A (Hwang, Holt, & Petre 2000) which reveal a few radially aligned, X-ray emission "streamers" along the western limb, opposite of the jet.

A broad axial asymmetry with narrow and opposing areas of high-speed ejecta bears similarities with core-collapse explosions recently modeled using collimated polar jets (Blackman & Yi 1998; Khokhlov et al. 1999; Höflich, Wheeler, & Wang 1999; MacFadyen & Woosley 1999). The fact that the highest velocity ejecta show S, Ar dominated spectra is consistent with these models where the innermost layers are ejected with the highest velocities. Moreover, these models suggest a fairly uniform expansion away from the jets, much like that implied by the NKs. Unfortunately, the current Cas A outer knot data set does not allow determining if the asymmetry here is truly axisymmetric and in which directions since, as discussed above (§ 4.1), optical knot visibility appears enhanced near the plane of the sky.

Jet-induced explosions, however, are not the only way to create highly asymmetrical expansions, and available kinematic data on the remnant's main shell do not point to a simple bipolar expansion. Cas A's bright optical shell exhibits a pronounced, multiring like three-dimensional structure (Reed et al. 1991; Lawrence et al. 1995; J. E. Reed 1998, private communication). The nature of these large rings is unknown but could be related to expanding ^{56}Ni bubbles (Chevalier 2000). Such a highly asymmetric structure of the remnant's 4000–6000 km s^{-1} ejecta along with an even more complex bubble-like texture seen in the radio (Braun, Gull, & Perley 1987) implies a complex explosion asymmetry resembling multiple high-speed fingers of emerging mantle ejecta (Burrows, Hayes, & Fryxell 1995; Janka & Müller 1996). Nonetheless, there are hints that some of these main shell rings could still be related to jetlike streams of higher velocity debris since one of them lies at the base of the northeastern jet.

An asymmetrical explosion of the Cas A SN might help explain the stronger than expected ^{44}Ti gamma-ray line detection at 1.157 MeV from COMPTEL and OSSE aboard the *Compton Gamma Ray Observatory* (GRO) (Iyudin et al. 1994; Iyudin et al. 1997; The et al. 1996; Dupraz et al. 1997). These observations indicate a gamma-ray line flux around 3.5×10^{-5} photons cm^{-2} s^{-1} indicating a ^{44}Ti mass $\simeq 1 \times 10^{-4}$ $M_{\odot}$. This mass is larger than the 0.6–8.0 $\times 10^{-5}$ $M_{\odot}$ predicted by high-mass supernova models (Woosley & Weaver 1995; Thielemann, Nomoto, & Hashimoto 1996).

If accompanied by a predicted ≥ 0.05 $M_{\odot}$ of ^{56}Ni, the Cas A supernova should have had a peak visual brightness of around -4 mag assuming no visual extinction. To explain Flamsteed's 6 mag observation of 3 Cassiopeia requires then $\sim$10 mag of extinction (Timmes et al. 1996) which is much greater than the 4–8 mag estimated for the remnant (Troland, Crutcher, & Helies 1985; Hurford & Fesen 1996). However, Nagataki et al. (1998) has shown that axisymmetric collapse-driven explosions can produce an enhancement of the ^{44}Ti/^{56}Ni ratio needed to explain the ^{44}Ti mass implied by the GRO observations without creating more ^{56}Ni making the SN too bright to be consistent with the lack of more historical sightings. Although other solutions have been suggested (Mochizuki et al. 1999) and there well could be increased extinction toward Cas A's explosion point due to small molecular cloud clumps (Goss, Kalberla, & Dickel 1984; Troland, Crutcher, & Helies 1985), the expansion asymmetry indicated by the NE jet and other outlying S, O, Ar debris is consistent with the Nagataki et al. (1998) explanation.

An asymmetrical explosion is also likely to induce substantial interlayer turbulence and, indeed, the remnant's bright main shell exhibits several properties indicating strong internal mixing. Chevalier & Kirshner (1979) argued that some nonspherical motions must have occurred in the Cas A SN due to the lack of correlated knot abundances and expansion velocity. Similarly, Winkler, Roberts, & Kirshner (1991) reported finding a wide range of main shell O and S abundances spanning more than an order of magnitude. From their data, Winkler et al. concluded that the "inner core of the progenitor was mixed by the supernova with overlying material, at least as far out as the oxygen zone."

Cas A exhibits unusual abundances relative to other so-called oxygen-rich remnants (van den Bergh 1988) particularly in showing an apparent lack of neon and magnesium (see Fesen 1990; Vink, Kaastra, & Bleeker 1996). This has been used to argue against mixing (Johnson & Yahil 1984). However, filaments with strong neon emission have now been detected in the mid-infrared (Douvion et al. 1999), and the analysis of *Chandra* X-ray data by Hughes et al. (2000) lends strong supporting evidence for a turbulent explosion of the Cas A SN. Hughes et al. found bright X-ray knots to be composed of explosive O-burning products mixed together with less metal-rich material from H, He, N-rich layers farther out in radius. Diffuse Fe-rich X-ray emitting material, presumably from explosive S-rich innermost layers, was found lying outside the S-rich material suggesting a spatial inversion of significant portions of the SN during the explosion.

Finally, the notion that Cas A exploded asymmetrically is in-line with increasing observational evidence for asymmetrical explosions in core-collapse SNe. The early detection of radioactive products in SN 1987A (Kumagai et al. 1989; Tueller et al. 1991; McCray 1993), asymmetrical line profiles in SN 1993J (Spyromilio 1994; Wang & Hu 1994), and significant polarizations in Type II SNe (Mèndez et al. 1988; Jeffrey 1991) have often been cited as evidence for mixing of the ejected material. Our detections now of mixed emission knots (MEKs) along Cas A's east and west limbs with velocities greater than most NKs lend support for some degree of turbulent mixing possibly due to mass

entrainment. This statement is true regardless of whether the MEKs are micro- or macroscopically mixed.

5. CONCLUSIONS

Our survey of faint, optical emission around the outer periphery of the Cas A remnant has revealed over two dozen new [N II] emission knots as well as the first detections of outlying O + S bright ejecta (FMKs) outside of the NE jet. Combined with previous studies, there are now some 75 optical knots outside the remnant's main shell, excluding the 100+ FMKs located in the NE jet. These new detections make it clear that outer knots, albeit faint, constitute a significant population of SN debris representing the highest velocity ejecta. Moreover, these knots appear both chemically and kinematically distinct from the remnant's bright, optical emission shell.

Specific results and conclusions are as follows:

1. Twenty-five new outlying knots have been detected which show a 4500–7500 Å spectrum dominated by [N II] $\lambda\lambda$6583,6548 line emission (NKs). This brings to 50 the number of this type of ejecta now known. Most lie within an expansion velocity band of 8000 and 10,000 km s^{-1}. Several knots along the remnant's eastern limb appear to be interacting with a local H II region and thus may have experienced significant decelerations. When deceleration effects are taken into account, a nearly isotropic ejection velocity $\simeq$10,000 km s^{-1} is suggested. A handful of knots located in the southwest are striking exceptions, possessing velocities up to 12,000 km s^{-1}. N-rich ejecta fragments are presumably shrapnel from the He, N-rich outer layers of the Cas A progenitor. The presence of appreciable hydrogen emission in just three out of 50 knots suggests a hydrogen poor photosphere at the time of supernova outburst.

2. Nearly 20 new outlying O + S rich fast moving knots are discovered, mostly along the remnant's western limb. These are the first to be found outside of the main shell not associated with the northeast jet and indicate a much wider distribution of high-velocity O + S debris than previously realized. The new ejecta knots possess space velocities between 7600 and 12,600 km s^{-1}. Ejecta showing strong sulfur emissions but weak or absent oxygen lines dominate the highest velocity debris ($\geq$11,000 km s^{-1}). This suggests an expansion in which the innermost S-rich layers were somehow ejected up through overlying material, with final outward velocities even higher than debris from the N-rich photosphere. The detection of such sulfur dominated ejecta only along the northeast and southwest limbs suggests a highly asymmetrical expansion, possibly bipolar. Such an asymmetrical expansion might have led to some of the strong mixing observed in the main shell.

3. Three new "mixed" N + O, S, Ar type knots (MEKs) have been found along the remnant's western limb. These lie near the newly discovered western O, S, Ar emission knots (FMKs) and nearly opposite of the NE jet, the only previously known region having MEK type knots. Although all line emissions in each knot exhibit the same radial velocities, the true nature of these "mixed" ejecta is uncertain. Higher spatial resolution images along with follow-up spectra are needed to determine whether these knots are really homogeneously mixed ejecta or simply closely packed clusters of chemically distinct NK/FMK debris. Nonetheless, the presence of N-rich material with S, Ar-rich ejecta along both east and west limbs having velocities $\geq$10,000 km s^{-1} suggests significant turbulent layer mixing, possibly as a result of high-speed mass entrainment.

4. All 75 outer knots discussed lie ahead of the remnant's forward shock front, meaning they are moving through local undisturbed, unshocked CSM or ISM. Detection of NKs and FMKs in groups or small clusters in particular regions suggests the presence of extended CSM and/or ISM of sufficient density is required for creating strong internal shocks thereby making them optically visible. The majority of all outlying knots lie within $\pm 20^{\circ}$ of the plane of the sky, suggesting a near tangent viewing angle is an important additional factor in determining optical visibility.

5. A few optical/radio/X-ray emission coincidences are identified along the southeastern limb at the locations of some outlying optical knots. A bright, radio filamentary arc located just outside the remnant's northern shell shows faint, diffuse optical emission. This optical emission may be a reflection nebula associated with a IR detected CSM/ISM cloud whose dust is scattering the bright [S II], [O I], and [O II] line emissions of Cas A's bright northern optical ejecta.

6. A compact, neighboring radio feature farther to the north may be related to some of the newly discovered high-velocity, outlying optical knots. A faint, bow-shaped cone of outermost emission with a bright knot at its northern apex has been attributed to clumps of intermediate velocity debris puncturing a decelerated shell created by formerly higher speed ejecta (Braun, Gull, & Perley 1987). We suggest, instead, it is a cluster of outlying ejecta knots like that seen elsewhere around the remnant but made more visible in the radio due to their passage through the northern edge of the local CSM/ISM cloud. The projected space velocity displacements for several nearby NK type knots are equal to that of the feature's bright apex.

Future studies of the remnant's highest velocity debris promise further kinematic and chemical information. Besides a detailed quantitative chemical analysis of the various types of outer ejecta using metal-rich shock models, future work might include a much deeper search for high-speed debris using the near infrared lines of He I 10830 Å and [S II] $\lambda\lambda$10,300–10,500 for NK and FMK ejecta, respectively. Uncovering many more emission knots, particularly along the high-extinction west limb region, will help better define this young remnant's global kinematics and structure.

We are grateful to R. Barr and the MDM staff for their excellent assistance in instrument setup and preparation, S. van den Bergh for helpful comments and suggestions, and the referee for a careful reading of the manuscript. We thank B. Koralesky and L. Rudnick for the 20 cm VLA radio image, G. Allen and R. Petre for a *ROSAT* image, and D. Patnaude for the *Chandra* images of Cas A. We also thank A. Hurford and C. Gerardy for help in obtaining some of the spectroscopic data, Y. E. Koms for general observer support, and the gracious hospitality of the William B. Hanson Center for Space Sciences at UT Dallas where much of this paper was written.

APPENDIX A

NOTES ON INDIVIDUAL KNOTS

2.—Images taken in 1998 taken using a 6510 Å filter show a $\simeq 2''$ long emission knot extended in the radial direction away from the center of expansion (see Fig. 2*b*).

3.—This knot appears to have faded considerably over the last decade, being easily detectable in broad Hα images taken in 1985 (see FBB) but was only barely visible in 1996 (Fig. 2*a*). Knot does not show up in 1998 Hα minus 6510 Å difference image (Fig. 2*b*) despite its similar radial velocity to Knot 2 which was easily detected.

3A.—High proper motion confirmed through comparison of 1996 Hα image and several 1985 images published by FBB covering the Knot 1–3 region (see Figs. 3 and 4 in FBB).

3B.—High proper motion confirmed through comparison of 1996 Hα image and the 1992 Hα image of Fesen & Gunderson (1996).

6A.—High proper motion confirmed through comparison of 1996 Hα image and the 1985 image published by FBB covering the Knot 4–6 region (see their Fig. 7).

9A,B.—Best resolution images show at least two closely spaced knots about 1″–1.″5 apart. We have designated the outermost one 9A, with 9B following. Spectroscopic data refer to the blend of both knots. These knots are visible on archival Palomar plates.

10.—Visible on archival Palomar plates. Deep 1996 Hα images hints at some faint trailing emission.

10A.—Knot was not detected by FBG due to coincident position with nearby faint star in 1986.

12.—High proper motion confirmed through comparison of 1996 Hα image and the 1986 image published by FBG covering the Knot 12 region (see their Fig. 2).

12A, 12B.—High proper motions suspected through comparison of 1996 Hα image and the 1985 and 1986 images of FBB and FBG. Complex emission structure in earlier frames prevents a clear knot identification.

13.—This emission knot described by FBG could not be confidently identified on the 1996 images/spectra or connected to Knots 13A–D. A faint patch of Hα emission appears coincident with Knots 13A–D (Fesen & Gunderson 1996; their Fig. 11).

14A.—A streak of emission about 3″ long with a bright end facing the remnant's center. Detected in 1998 via 6510 Å imaging along with Knots 15B and 15C.

15.—Also known as KB 91 (Kamper & van den Bergh 1976). Easily visible on a 1958 Palomar 5 m plate (see van den Bergh & Dodd 1970). Brightness does not appear to have significantly changed over past $\simeq 40$ years.

15A.—High proper motion confirmed through comparison of our 1996 broad [S II] image and the 1992 [S II] image of Fesen & Gunderson. May have brightened significantly during the past year since the measured 1997.8 flux is more than twice that estimated in 1996.7.

16, 16A, 17, 17A, 17B.—No proper motion information due to a lack of reliable knot detection/identification on archival published images. Knot 17B appears extended ($\simeq 2.''5$) and shows up strongly on [S II] images.

19.—Discovered by Kamper & van den Bergh (1991), this mixed emission type knot exhibits a starlike appearance and is one of the remnant's brighter outlying knots. Analysis of 1996 [S II] frames indicates a knot size of $\leq 0.''9$ suggesting a true dimension of ≤ 0.015 (d/3.4 kpc) pc. This knot is easily seen on deep 1976 and 1983 *R*-band images (van den Bergh & Kamper 1985) but is not visible on Minkowski's 1958 103aF + RG2 plate (see van den Bergh & Dodd 1970; Fig. 1).

21A and 21D.—Collectively called "FMF_2" by Fesen & Gunderson (1996) (see their Fig. 2).

24 and 24A.—Only the [N II] λ6583 line detected well with only hint of the λ6548 line. Weak Hα emission ($v \sim 0$ km s^{-1}) detected spatially coincident with emission from these knots.

25.—Relatively bright SW emission patch visible in [S II]. High proper motion confirmed through comparison of 1996 [S II] and the 1992 [S II] image of Fesen & Gunderson.

27.—Weakly visible on 1958 broadband red plate (see van den Bergh & Dodd 1970) as a short filament. Its $216'' \pm 1.''5$ distance from the remnant's kinematic center of expansion (Kamper & van den Bergh 1976) on this plate suggests a proper motion of $0.''76 \pm 0.''04$ per year and a Cas A explosion date no earlier than 1674 ± 15.

61–63, 65, and 65.—NK knots located in the NE jet region (Fesen & Gunderson 1996). Quoted distances from remnant center are remeasured values off 1996 image data.

66A.—Called "FMF_1" by Fesen & Gunderson (1996) (see their Fig. 2).

82A and 82B.—Called "MEK_1" and "MEK_2" by Fesen & Gunderson (1996) (see their Fig. 2).

APPENDIX B

In their study of FMKs and MEKs in Cas A's northeast jet, Fesen & Gunderson (1996) listed 1988 epoch radial distances along with the implied space velocities assuming a remnant distance of 3 kpc. In order to update these values, as well as correct a few tabulation errors in listed radial distances (e.g., Knots 40–45) we remeasured the radial distances and recalculated the implied space velocities for these jet knots.

Listed below is a retabulation of radial distances and inferred space velocity values for all 87 knots in Cas A's northeast jet discussed by Fesen & Gunderson (1996). Table 5 lists 1996.7 epoch radial displacements from van den Bergh and Kamper's quoted center of expansion along with revised space velocities adopting Reed et al.'s derived 3.4 kpc distance and a 316 yr expansion age (t_o = A.D. 1680). These updated values for jet FMKs were those used in Figure 9*d*.

TABLE 5

EMISSION KNOTS IN THE NORTHEASTERN JET[a]

Knot ID	Knot Type	R^b (arcsec)	V_T^c (km s^{-1})	V_R (km s^{-1})	V_{Space} (km s^{-1})	Knot ID	Knot Type	R^b (arcsec)	V_T^c (km s^{-1})	V_R (km s^{-1})	V_{Space} (km s^{-1})
1	FMK	283	14400	+280	14400	41	FMK	99	5000	−2300	5500
2	FMK	262	13400	−160	13400	42	FMK	83	4200	+1520	4500
3	FMK	254	13000	−110	13000	43	FMK	80	4100	+1110	4300
4	FMK	241	12300	−120	12300	44	FMK	80	4100	−2780	4900
5	MEK	236	12000	−20	12000	45	FMK	75	3800	+20	3800
6	MEK	229	11700	+370	11700	46	FMK	249	12600	−1110	12700
7	FMK	227	11600	+350	11600	47	FMK	249	12600	−950	12700
8	FMK	220	11200	+420	11200	48	FMK	221	11300	−2290	11500
9	MEK	213	10900	+400	10900	49	MEK	220	11200	−1380	11300
10	MEK	212	10800	+450	10800	50	FMK	214	10900	−1360	11000
11	FMK	204	10400	+300	10400	51	FMK	208	10600	−1800	10800
12	FMK	196	10000	+420	10000	52	FMK	205	10500	−710	10500
13	FMK	188	9500	−380	9500	53	FMK	205	10500	−2330	10700
14	FMK	187	9500	+1040	9600	54	FMK	202	10300	−470	10300
15	FMK	171	8700	+2870	9200	55	FMK	190	9700	−700	9700
16	FMK	168	8500	+2800	9000	56	FMK	185	9400	−850	9500
17	FMK	97	4900	−1900	5300	57	FMK	185	9400	−2670	9800
18	FMK	93	4800	+2300	5300	58	FMK	181	9200	−800	9200
19	FMK	90	4600	+1400	4800	59	FMK	178	9100	−890	9100
20	FMK	88	4500	−2350	5100	64	FMK	95	4800	+2310	5300
21	FMK	83	4300	+1100	4400	67	FMK	100	5100	+2360	5600
22	FMK	83	4300	−2380	4900	68	FMK	98	5000	+940	5100
23	FMK	242	12400	−530	12400	69	FMK	92	4700	−2090	5100
24	FMK	238	12100	−530	12100	70	FMK	92	4700	+1120	4800
25	FMK	209	10600	−570	10600	71	FMK	84	4300	+3280	5400
26	MEK	199	10200	−2090	10400	72	MEK	217	11100	−420	11100
27	FMK	198	10100	−510	10100	73	MEK	229	11700	+210	11700
28	FMK	196	10000	−700	10000	74	FMK	240	12200	−420	12200
29	FMK	191	9700	−650	9800	75	FMK	218	11100	−110	11100
30	FMK	180	9200	−2150	9400	76	FMK	224	11400	−110	11400
31	FMK	174	8900	−2200	9200	77	FMK	226	11500	+290	11500
32	MEK	169	8600	−3250	9200	78	FMK	225	11500	−200	11500
33	FMK	168	8600	−2130	8800	79	FMK	230	11700	+110	11700
34	MEK	159	8100	−3200	8700	80	FMK	241	12300	−1340	12400
35	FMK	159	8100	−2400	8400	81	FMK	182	9300	+220	9300
36	MEK	149	7600	−3750	8500	83	FMK	183	9300	−300	9300
37	FMK	149	7600	−3100	8200	84	FMK	185	9500	−2450	9800
38	FMK	129	6600	−3200	7300	85	FMK	186	9500	−2210	9700
39	FMK	115	5900	−2450	6400	86	FMK	235	12000	+720	12000
40	FMK	109	5600	−2400	6100	87	FMK	275	14000	+190	14000

NOTE.—Table 5 is also available in machine-readable form in the electronic edition of the *Astrophysical Journal*.

[a] Knot ID numbers and radial velocities taken from Fesen & Gunderson 1996.

[b] Estimated 1996.7 radial distance from $\alpha[2000] = 23^h23^m27^s.7$, $\delta[2000] = 58°48'47''$.

[c] Transverse velocities calculated assuming $d = 3.4$ kpc and a 316 yr expansion age.

REFERENCES

Anderson, M. C., Jones, T. W., Rudnick, L., Tregillis, I. L., & Kang, H. 1994, ApJ, 421, L31
Anderson, M. C., & Rudnick, L. 1995, ApJ, 441, 307
———. 1996, ApJ, 456, 234
Ashworth, W. B. 1980, J. Hist. Astron., 11, 1
Baade, W., & Minkowski, R. 1954, ApJ, 119, 206
Bell, A. R., Gull, S. F., & Kenderdine, S. 1975, Nature, 257, 463
Bieging, J. H., & Crutcher, R. M. 1986, ApJ, 310, 853
Blackman, E. G., & Yi, I. 1998, ApJ, 498, L31
Braun, R., Gull, S. F., & Perley, R. A. 1987, Nature, 327, 398
Burrows, A., Hayes, J., & Fryxell, B. A. 1995, ApJ, 450, 830
Chevalier, R. A. 2000, preprint
Chevalier, R. A., & Kirshner, R. P. 1978, ApJ, 219, 931
———. 1979, ApJ, 233, 154
Dickel, J. R., Murray, S. S., Moris, J., & Wells, D. C. 1982, ApJ, 257, 145
Douvion, T., Lagage, P. O., & Césarsky, C. J. 1999, A&A, 352, L111
Dupraz, C., Bloemen, H., Bennett, K., Diehl, R., Hermsen, W., Iyudin, A. F., Ryan, J., & Schoenfelder, V. 1997, A&A, 324, 683
Fabian, A. C., Willingale, R., Pye, J. P., Murray, S. S., & Fabbiano, G. 1980, MNRAS, 193, 175
Fesen, R. A. 1990, AJ, 99, 1904
Fesen, R. A., & Becker, R. H. 1991, ApJ, 371, 621 (FB91)
Fesen, R. A., Becker, R. H., & Blair, W. P. 1987, ApJ, 313, 378 (FBB87)
Fesen, R. A., Becker, R. H., & Goodrich, R. 1988, ApJ, 329, L89 (FBG88)
Fesen, R. A., & Gunderson, K. S. 1996, ApJ, 470, 967 (FG96)
Filippenko, A. V. 1997, ARA&A, 35, 309
Garcia-Segura, G., Langer, N., & Mac Low, M.-M. 1996, A&A, 316, 133
Goss, W. M., Kalberla, P. M. W., & Dickel, H. R. 1984, A&A, 139, 317
Gotthelf, E. V., Koralesky, B., Hwang, U., Petre, R., Jones, T. W., Rudnick, L., & Holt, S. 1999, BAAS, 195, 112.06
Hamilton, A. J. S. 1985, ApJ, 291, 523
Höflich, P., Wheeler, J. C., & Wang, L. 1999, ApJ, 521, 179
Hogg, D. E., Macdonald, G. H., Conway, R. G., & Wade, C. M. 1969, AJ, 74, 1206
Hughes, J. P., Rakowski, C. E., Burrows, D. N., & Slane, P. O. 2000, ApJ, 528, 109
Hurford, A. P., & Fesen, R. A. 1996, ApJ, 469, 246
Hwang, U., Holt, S. S., & Petre, R. 2000, ApJ, 537, L119
Iyudin, A. F., et al. 1994, A&A, 284, L1

Iyudin, A. F., et al. 1997, in The Transparent Universe: Proc. Second INTEGRAL Workshop, ed. C. Winkler, T. J.-L. Courvoisier, & Ph. Durouchoux (ESA SP-382; Noordwijk: ESA), 142
Jank, H. T., & Müller, E. 1996, A&A, 306, 167
Jansen, F., Smith, A., Bleeker, J. A. M., de Korte, P. A. J., Peacock, A., & White, N. E. 1988, ApJ, 331, 949
Jeffrey, D. J. 1991, ApJ, 375, 264
Johnson, M. D., & Yahil, A. 1984, ApJ, 285, 587
Kamper, K., & van den Bergh, S. 1976, ApJS, 32, 351
———. 1991, BAAS, 23, 821
Keohane, J. W., Rudnick, L., & Anderson, M. A. 1996, ApJ, 466, 309
Kirshner, R., & Chevalier, R. A. 1977, ApJ, 218, 142
Khokhlov, A. M., Hoflich, P. A., Oran, E. S., Wheeler, J. C., Wang, L., & Chtchelkanova, A. Yu. 1999, ApJ, 524, L107
Koralesky, B., Rudnick, L., Gotthelf, E. V., & Keohane, J. W. 1998, ApJ, 505, L27
Kumagai, S., Shigeyama, T., Nomoto, K., Itoh, M., Nishimura, J., & Tsuruta, S. 1989, ApJ, 345, 412
Langer, N., & El Eid, M. F. 1986, A&A, 167, 265
Lagage, P. O., Claret, A., Ballet, J., Boulanger, F., Césarsky, C. J., Césarsky, D., Fransson, C., & Pollock, A. 1996, A&A, 315, L273
Lawrence, S. S., MacAlpine, G. M., Uomoto, A., Woodgate, B. E., Brown, L. W., Oliversen, R. J., Lowenthal, J. D., & Liu, C. 1995, AJ, 109, 2635
MacFadyen, A., & Woosley, S. E. 1999, ApJ, 524, 262
Massey, P., & Gronwald, C. 1990, ApJ, 358, 344
McCray, R. 1993, ARA&A, 31, 175
Mèndez, M., Clocchiatti, A., Benvenuto, G., Feinsten, C., & Marraco, U. G. 1988, ApJ, 334, 295
Minkowski, R. 1959, in Paris Symposium on Radio Astronomy, ed. R. N. Bracewell (Palo Alto: Stanford Univ. Press), 315
———. 1968, in Stars and Stellar Systems, 7, 623
Mochizuki, Y., Takahashi, K., Janka, H.-Th., & Diehl, R. 2000, A&A, 346, 831
Nagataki, S., Hashimoto, M.-A., Sato, K., Yamada, S., & Mochizuki, Y. S. 1998, ApJ, 492, L45
Oke, J. B. 1974, ApJS, 27, 21
Osterbrock, D. E., & Martel, A. 1992, PASP, 104, 76
Parenago, P. P., & Shklovsky, I. S. 1952, Astron. Tsirk., 131, 1
Peimbert, M., & van den Bergh, S. 1971, ApJ, 167, 223
Reynoso, E. M., Goss, W. M., & Dubner, G. M., Winkler, P. F., & Schwarz, U. J. 1997, A&A, 317, 203
Reber, G. 1944, ApJ, 100, 279
Reed, J. E., Hester, J. J., Fabian, A. C., & Winkler, P. F. 1991, BAAS, 23, 826
———. 1995, ApJ, 440, 706
Ryle, M., Elsmore, B., & Neville, A. C. 1965, Nature, 205, 1259
Ryle, M., & Smith, F. G. 1948, Nature, 162, 462
Schwarz, U. J., Goss, W. M., & Kalberla, P. M. W. 1997, A&AS, 123, 43
Searle, L. 1971, ApJ, 168, 41
Shklovsky, I. S. 1953, Soviet. Astron.–AJ, 266, 1952
Stone, R. P. S. 1977, ApJ, 218, 767
The, L.-S., et al. 1996, A&A, 120, 357
Spyromolio, J. 1994, MNRAS, 266, 61
Thielemann, F.-K., Nomoto, K., & Hashimoto, M. 1996, ApJ, 460, 408
Timmes, F. X., Woosley, S. E., Hartmann, D. H., & Hoffman, R. D. 1996, ApJ, 464, 332
Troland, T. H., Crutcher, R. M., & Heiles, C. 1985, ApJ, 298, 808
Tsunemi, H., Yamashita, K., Masai, K., Hayakawa, S., & Koyama, K. 1986, ApJ, 306, 248
Tueller, J., et al. 1991, ApJ, 351, L41
Tuffs, R. J. 1986, MNRAS, 219, 13
van den Bergh, S. 1971, ApJ, 165, 457
———. 1988, ApJ, 327, 156
van den Bergh, S., & Dodd, W. W. 1970, ApJ, 162, 485
van den Bergh, S., & Kamper, K. 1983, ApJ, 268, 129
———. 1985, ApJ, 293, 537
Vink, J., Bloemen, H., Kaastra, J. S., Bleeker, J. A. M. 1998, A&A, 339, 201
Vink, J., Kaastra, J. S., & Bleeker, J. A. M. 1996, A&A, 307, L41
Wang, L., & Hu, J. Y. 1994, Nature, 369, 380
Winkler, P. F., Roberts, P. F., & Kirshner, R. P. 1991, in Supernovae: The Tenth Santa Cruz Summer Workshop in Astronomy and Astrophysics, ed. S. E. Woosley (New York: Springer), 652
Woosley, S. E., & Weaver, T. A. 1995, ApJ, 448, 315